2900-371-T(I)

Report of Project MICHIGAN

OPTIMUM CHARACTERISTICS OF SOME MOTION-COMPENSATION SYSTEMS

Volume I

Theory and Application of Doppler-Inertial Systems

W. A. PORTER
A. Y. BILAL

March 1963

Navigation and Guidance Laboratory
Institute of Science and Technology
THE UNIVERSITY OF MICHIGAN
Ann Arbor, Michigan

NOTICES

Sponsorship. The work reported herein was conducted by the Institute of Science and Technology for the U. S. Army Electronics Command under Project MICHIGAN, Contract DA-36-039 SC-78801. Contracts and grants to The University of Michigan for the support of sponsored research by the Institute of Science and Technology are administered through the Office of the Vice-President for Research.

Note. The views expressed herein are those of Project MICHIGAN and have not been approved by the Department of the Army.

Distribution. Initial distribution is indicated at the end of this document. Distribution control of Project MICHIGAN documents has been delegated by the U. S. Army Electronics Command to the office named below. Please address correspondence concerning distribution of reports to:

Commanding Officer
U. S. Army Liaison Group
Project MICHIGAN
The University of Michigan
P. O. Box 618
Ann Arbor, Michigan

ASTIA Availability. Qualified requesters may obtain copies of this document from:

Armed Services Technical Information Agency
Arlington Hall Station
Arlington 12, Virginia

Final Disposition. After this document has served its purpose, it may be destroyed. Please do not return it to the Institute of Science and Technology.

PREFACE

Project MICHIGAN is a continuing, long-range research and development program for advancing the Army's combat-surveillance and target-acquisition capabilities. The program is carried out by a full-time Institute of Science and Technology staff of specialists in the fields of physics, engineering, mathematics, and psychology, by members of the teaching faculty, by graduate students, and by other research groups and laboratories of The University of Michigan.

The emphasis of the Project is upon research in imaging radar, MTI radar, infrared, radio location, image processing, and special investigations. Particular attention is given to all-weather, long-range, high-resolution sensory and location techniques.

Project MICHIGAN was established by the U. S. Army Signal Corps at The University of Michigan in 1953 and has received continuing support from the U. S. Army. The Project constitutes a major portion of the diversified program of research conducted by the Institute of Science and Technology in order to make available to government and industry the resources of The University of Michigan and to broaden the educational opportunities for students in the scientific and engineering disciplines.

Progress and results described in reports are continually reassessed by Project MICHIGAN. Comments and suggestions from readers are invited.

Robert L. Hess
Director
Project MICHIGAN

CONTENTS

FIGURES

TABLE

OPTIMUM CHARACTERISTICS OF SOME MOTION-COMPENSATION SYSTEMS
Volume I: Theory and Application of Doppler-Inertial Systems

ABSTRACT

A side-looking radar system employing synthetic-antenna techniques can obtain azimuth resolution finer than that afforded by the radar beamwidth. The capabilities of such systems depend in part on the accurate sensing of vehicle perturbation from a reference path and subsequent phase compensation for this motion.

This volume deals with the optimization, for such motion-compensation activities, of a family of doppler-inertial systems. By use of the variational calculus techniques of the Wiener filter theory, functional relationships between optimum system performance and sensor noise errors are developed, and systems with and without dynamically induced errors are compared.

1
INTRODUCTION

Over the past several years, high-resolution radar systems have rapidly advanced in sophistication. Unfortunately, this broad progress has been marred by pockets of technical depression. The technical problem of primary importance today is the development of sophisticated optimum motion-compensation systems with capabilities and performed profiles that remove the primary obstacle to a "really" high resolution system.

Although it has been recognized for several years that the inadequacies of the motion-compensation technology were the main stumbling block to high-resolution performance, curiously enough, no comprehensive analysis of motion-compensation systems has (until the present study) been undertaken. Past efforts on such systems were based partly or wholly upon ideas of system design adapted from navigation applications. These applications did not stress high-fidelity, instantaneous accuracy, but were mainly concerned with long-term average accuracy. As a consequence of the AN/UPD-1 (airborne high-resolution radar) program, new ideas on system design were found to be necessary. Development of new techniques, however, is an arduous task.

Furthermore, the navigational philosophy of system design has many idiosyncrasies within itself. These have resulted in a multitude of system forms, and hence confusion and delay in the implementation of effective research progress.

We still arbitrarily assume noise systems with known spectral forms and rely upon linear system analysis—two assumptions which run contrary to actual physical realities. The outlook is not completely

bleak, however. Although many new developments are still necessary, some progress has been made. The conclusions presented in Reference 1 and in this report are the first in a series of assaults on the problem. We hope that they will serve to guide present system developments and to measure future progress in the research programs that should follow.

2
SYSTEM REPRESENTATION

2.1. GENERAL BLOCK DIAGRAM

The seemingly endless variety of block diagrams usable for the description of doppler-inertial systems has its advantages. However, the design engineer many times is faced with such a diverse selection that the possibilities are bewildering. In this section, a systematic approach to system representation is presented with the following objectives: (1) to emphasize certain aspects which the author feels have not been completely understood; (2) to show that the motion-compensation application is compatible with the concept of generalized system optimization.

Figure 1 is a block diagram for the crosstrack channel of a D-I system. If a single accelerometer is to be used, this figure comprehends most of the possible methods for coupling the doppler and the inertial systems for motion-compensation applications. The notations used on Figure 1 are as follows:

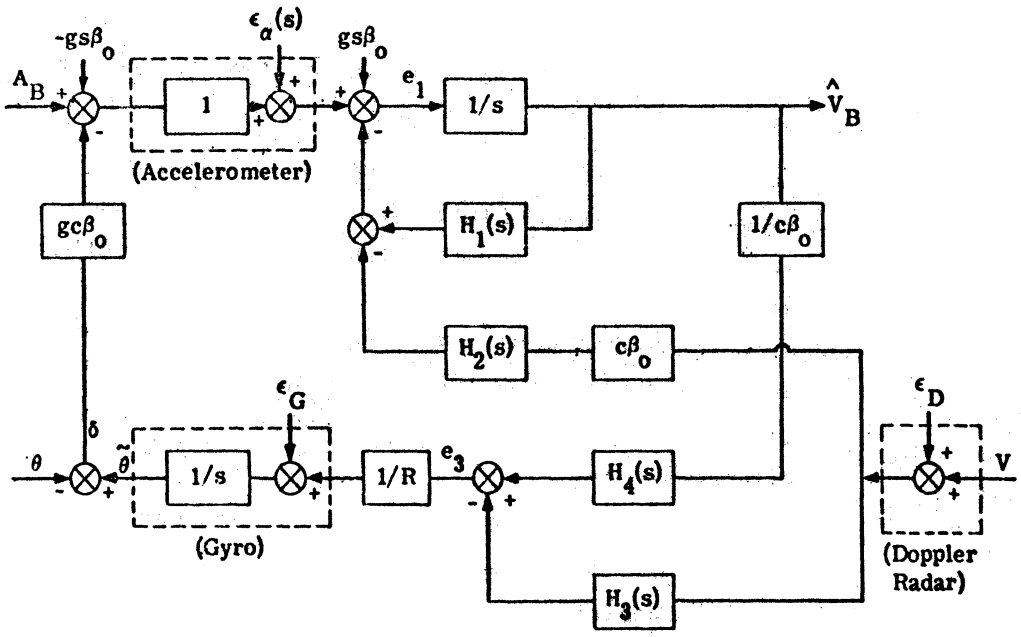

FIGURE 1. A GENERAL D-I SYSTEM

ϵ_α, ϵ_G, ϵ_D = accelerometer error, gyro drift rate, and doppler noise, respectively

δ = verticality error

g, R = gravity field and earth radius, respectively

β_o = accelerometer tilt angle from a level position

$s\beta_o$ and $c\beta_o$ = $\sin\beta_o$ and $\cos\beta_o$, respectively

$\hat{V}_B$, $\hat{\theta}$ = system estimates of along-the-beam velocity and verticality, respectively

A_B, θ = true along-the-beam acceleration and vertical direction, respectively

$\Omega = \sqrt{\frac{g}{R}}$

To illustrate the general nature of this block diagram, we will derive the various error equations and, by subsequent identification of the filter transfer functions $H_1(s)$, $H_2(s)$, $H_3(s)$, and $H_4(s)$, we will relate this system to the various possible forms.

2.1.1. ERROR ANALYSIS. Equations 1, 2, and 3 are derived from signal summation on Figure 1.

$$e_1(s) = \epsilon_\alpha(s) + A_B(s) - gc\beta_o\delta(s) - H_1(s)\hat{V}_B(s) + H_2(s)V_{ct}(s) + H_2(s)\epsilon_D(s) \tag{1}$$

$$\delta(s) = (1/s)\epsilon_G(s) + \left(\frac{1}{Rs}\right)e_3(s) - [V_{ct}(s)]/Rs \tag{2}$$

$$e_3(s) = \left[\frac{1}{c\beta_o}H_4(s)\right]\hat{V}_B(s) - H_3(s)V_{ct}(s) - H_3(s)\epsilon_D(s) \tag{3}$$

Since $\hat{V}_B(s)$ equals the integral of $e_1(s)$, it follows that

$$\hat{V}_B(s) = \frac{\epsilon_\alpha(s)}{s} + V_B(s) - \frac{gc\beta_o}{s}\delta(s) - [H_1(s)]\frac{\hat{V}_B(s)}{s} + \left[c\beta_o\frac{H_2(s)}{s}\right]V_{ct(s)} + \left[c\beta_o\frac{H_2(s)}{s}\right]\epsilon_D(s) \tag{4}$$

If we substitute Equations 2 and 3 into this expression, it follows that

$$\hat{V}_B(s)\left[1 + \frac{H_1(s)}{s} + \frac{\Omega^2}{s^2}H_4(s)\right] = \frac{\epsilon_\alpha(s)}{s} - \frac{gc\beta_o}{s}\epsilon_G(s) + \left[\frac{H_2(s)}{s} + \frac{\Omega^2}{s^2}c\beta_o H_3(s)\right]\epsilon_D(s) + V_B(s)$$

$$+ \left[c\beta_o\frac{H_2(s)}{s} + \frac{\Omega^2 c\beta_o}{s^2}H_3(s) + \frac{\Omega^2 c\beta_o}{s^2}\right]V_{ct}(s) \tag{5}$$

which may be reduced to

$$\hat{V}_B(s)\left[s^2 + sH_1(s) + \Omega^2 H_4(s)\right] = N(\epsilon, s) + s^2 V_B(s) + \left\{sH_2(s)c\beta_o + \Omega^2 c\beta_o[1 + H_3(s)]\right\} V_{ct}(s) \quad (6)$$

where the identification

$$N(\epsilon, s) = s\epsilon_\alpha(s) - gc\beta_o \epsilon_G(s) + \left[sH_2(s)c\beta_o + \Omega^2 c\beta_o H_3(s)\right] \epsilon_D(s) \quad (7)$$

has been made. Solving Equation 6 for $\hat{V}_B(s)$ yields

$$\hat{V}_B(s) = \frac{N(\epsilon, s)}{\left[s^2 + sH_1(s) + \Omega^2 H_4(s)\right]} + \frac{s^2 V_B(s) + \left\{sH_2(s)c\beta_o + \Omega^2 c\beta_o[1 + H_3(s)]\right\} V_{ct}(s)}{\left[s^2 + sH_1(s) + \Omega^2 H_4(s)\right]} \quad (8)$$

Since $\hat{V}_B(s)$ is an estimate of V_B, we identify the pertinent error in this quantity as $\hat{V}_B(s) - V_B(s)$; hence

$$E\hat{V}_B(s) = \hat{V}_B(s) - V_B(s) = \frac{N(\epsilon, s)}{\left[s^2 + sH_1(s) + \Omega^2 H_4(s)\right]}$$

$$+ \frac{-\left[sH_1(s) + \Omega^2 H_4(s)\right] V_B(s) + \left\{sH_2(s)c\beta_o + \Omega^2 c\beta_o[1 + H_3(s)]\right\} V_{ct}(s)}{\left[s^2 + sH_1(s) + \Omega^2 H(s)\right]} \quad (9)$$

Noting that $V_B(s) = c\beta_o V_{ct}(s) - s\beta_o V_Z(s)$ it follows that

$$E\hat{V}_B(s) = \frac{N(\epsilon, s)}{s^2 + sH_1(s) + \Omega^2 H_4(s)}$$

$$+ \frac{\left\{sH_2(s) + \Omega^2[1 + H_3(s)] - sH_1(s) - \Omega^2 H_4(s)\right\} c\beta_o V_{ct}(s) + s\beta_o \left[sH_1(s) + \Omega^2 H_4(s)\right] V_Z(s)}{s^2 + sH_1(s) + \Omega^2 H_4(s)} \quad (10)$$

We note that in Equation 10, $H_1(s)$ and $H_4(s)$, $H_2(s)$ and $H_3(s)$ occur in particular combination. In an attempt to simplify this notation, let us identify these combinations by the two filter forms $H_5(s)$ and $H_6(s)$ which will be defined as

$$H_5(s) = H_4(s) + \frac{s}{\Omega^2} H_1(s) \quad (11)$$

$$H_6(s) = H_3(s) + \frac{s}{\Omega^2} H_2(s) \quad (12)$$

Through this new notation, Equation 10 reduces to

$$E\hat{V}_B(s) = \frac{N(\epsilon, s)}{s^2 + \Omega^2 H_5(s)} + \Omega^2 \frac{\left[H_5(s) + H_6(s) + 1\right] c\beta_\sigma V_{ct}(s) + H_5(s) s\beta_o V_Z(s)}{s^2 + \Omega^2 H_5(s)} \tag{13}$$

2.1.2. RELATED SYSTEM FORMS. The various forms of system configuration under consideration for purposes of motion compensation can now be identified as particular members of the family of systems depicted in Figure 1. This point can be illustrated by use of Table I, which presents all system forms, ranging from pure inertial with level accelerometer to a completely coupled doppler inertial with tilted accelerometer. The conclusion to be drawn from this display of systems is simply that Figure 1 has sufficient mobility to represent this broad scope of systems. A less complicated block diagram would be more convenient, however, provided this mobility is not lost. The present diagram can be simplified by consideration of Equations 11 and 12 of the last section, which show that it is not necessary to have 4 independent filters. As a matter of fact, $H_1(s)$ and $H_2(s)$ in Figure 1 can be omitted if $H_3(s)$ and $H_4(s)$ take on the forms of $H_5(s)$ and $H_6(s)$. Furthermore, if we are interested in minimizing the error effects of true crosstrack motion, a glance at Equation 13 suggests the auxiliary constraint

$$H_5(s) + H_6(s) + 1 = 0 \tag{14}$$

In this case, Figure 1 reduces to either one of the two particular forms depicted in Figures 2 and 3, where

$$Q(s) = H_5(s)$$

$$H(s) = H_6(s)$$

Since these two forms represent identical systems, the form which leads to the simplest error equations can be selected. This form is shown in Figure 2. We should note here that it is quite similar to the block diagram used in Reference 1, where theoretical optimization studies have been carried out both with and without the constraint of Equation 14. For Figure 2, the pertinent error equation then becomes

$$E\hat{V}_B(s) = \frac{N[\epsilon, Q(s)] + \Omega^2 s\beta_o Q(s) V_Z(s)}{s^2 + \Omega^2 Q(s)} \tag{15}$$

where the identification

$$N[\epsilon, Q(s)] = s\epsilon_\alpha(s) - gc\beta_o \epsilon_G(s) - \Omega^2 c\beta_o (1 - Q)\epsilon_D(s) \tag{16}$$

has been used.

TABLE I. SYSTEM IDENTIFICATION

Case	$H_1(s)$	$H_2(s)$	$H_3(s)$	$H_4(s)$	β_o	EV_B	Type
I	0	0	0	1	0	$\frac{s\epsilon_\alpha(s) - g\epsilon_G(s)}{s^2 + \Omega^2}$	Pure Inertial
II	γ	0	0	1	0	$\frac{s\epsilon_\alpha(s) - g\epsilon_G(s) - s\gamma V_{ct}(s)}{s^2 + \gamma s + \Omega^2}$	Pure Inertial Self-damped
III	γ	0	0	K	0	$\frac{s\epsilon_\alpha(s) - g\epsilon_G(s) + [\Omega^2(1 - K) - s\gamma]V_{ct}(s)}{s^2 + \gamma s + K\Omega^2}$	Self-damped & Detuned
IV	γ	γ	K	1 + K	0	$\frac{s\epsilon_\alpha(s) - g\epsilon_G(s) + (s\gamma + \Omega^2 K)\epsilon_D(s)}{s^2 + \gamma s + \Omega^2(1 + K)}$	Doppler Damped & Detuned
V	$H_1(s)$	0	0	$H_4(s)$	β_o	$\frac{(s\epsilon_\alpha(s) - gc\beta_o\epsilon_G(s)) + c\beta_o\left[-sH_1(s) + \Omega^2(1 - H_4(s))\right]V_{ct}(s)}{s^2 + sH_1(s) + \Omega^2 H_4(s)}$ $+ \frac{s\beta_o\left[sH_1(s) + \Omega^2 H_4(s)\right]V_Z(s)}{s^2 + sH_1(s) + \Omega^2 H_4(s)}$	Tilted Self-damped & Detuned
VI	$H_1(s)$	$H_1(s)$	$H_3(s)$	$1 + H_3(s)$	β_o	$\frac{s\epsilon_\alpha(s) - gc\beta_o\epsilon_G(s) + \left[sH_1(s) + \Omega^2 c\beta_o H_3(s)\right]\epsilon_D(s)}{s^2 + sH_1(s) + \Omega^2[1 + H_3(s)]}$ $\frac{sH_1(s)(1 - c\beta_o)V_{ct}(s)}{s^2 + sH_1(s) + \Omega^2[1 + H_3(s)]}$ $+ \frac{\left[sH_1(s) + \Omega^2(1 + H_3(s))\right]s\beta_o V_Z(s)}{s^2 + sH_1(s) + \Omega^2[1 + H_3(s)]}$	Tilted Doppler Damped & Tuned

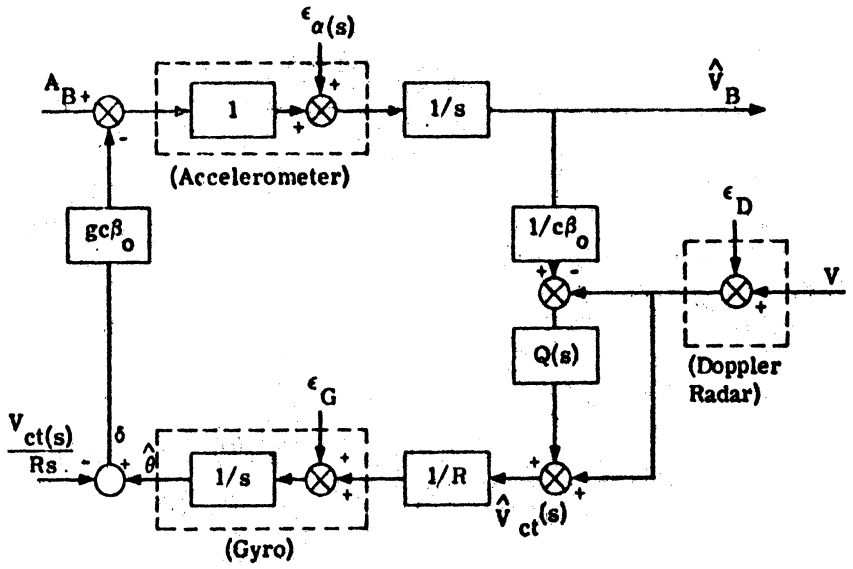

FIGURE 2. ALTERNATIVE D-I SYSTEM, FORM #1

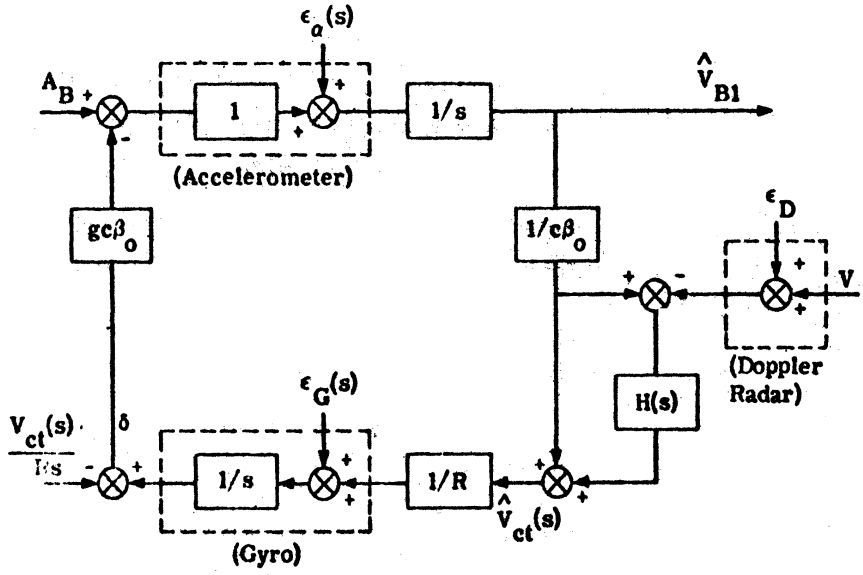

FIGURE 3. ALTERNATIVE D-I SYSTEM, FORM #2

In the above reference, it was found convenient to introduce the filter form

$$I(s) = \frac{\Omega^2 Q(s)}{s^2 + \Omega^2 Q(s)} \tag{17}$$

In terms of I(s), Equation 15 reduces to

$$\hat{EV}_B(s) = [1 - I(s)]\epsilon_\alpha(s) + I(s)\epsilon_b(s) \tag{18}$$

where

$$\epsilon_\alpha(s) = \frac{1}{s^2}\left[s\epsilon_\alpha(s) - gc\beta_o\epsilon_G(s) - \Omega^2 c\beta_o\epsilon_D(s)\right] \tag{19}$$

$$\epsilon_b(s) = \epsilon_D(s) + s\beta_o V_2(s) \tag{20}$$

In partial summary, we have demonstrated that a wide range of systems (a few of which are listed in Table I) can be discussed or described in terms of the generalized notation of Equations 15 and 18 and/or Figures 1 and 2. The following sections will show that: 1) understanding of these systems is enhanced by this approach; and 2) more importantly, failure to approach system selection in this manner can lead to false conclusions.

2.2. SECOND-ORDER/THIRD-ORDER DILEMMA

An unfortunate side effect of the unsystematic description of D-I systems is the number of ambiguities in the current nomenclature of certain systems. For instance, the use of the terms "second order" and "third order" (to designate the familiar configuration shown in Figure 4) is inaccurate. This terminology derives from the fact that the characteristic equations of those two specific systems are of order 2 and 3 respectively. However, we shall show in the following sections that there are a number of possible second-order systems, each with distinguishing characteristics.

Let us begin by defining a second-order system as a system whose characteristic equation has the form $s^2 + \gamma s + (1 + a)\Omega^2$. For instance, the error equation of Figure 4 is given by

$$E_V(s) = \frac{-g\epsilon_G(s) + s\epsilon_\alpha(s) + (\gamma s + \alpha\Omega^2)\epsilon_D(s)}{s^2 + \gamma s + (1 + \alpha)\Omega^2} \tag{21}$$

This error equation describes system performance when, as is common practice, the calculated velocity is taken directly from the output of the integrator. However, let us select our output from another spot in the system. For instance, as shown in Figure 5, the output of the accelerometer may be fed to a

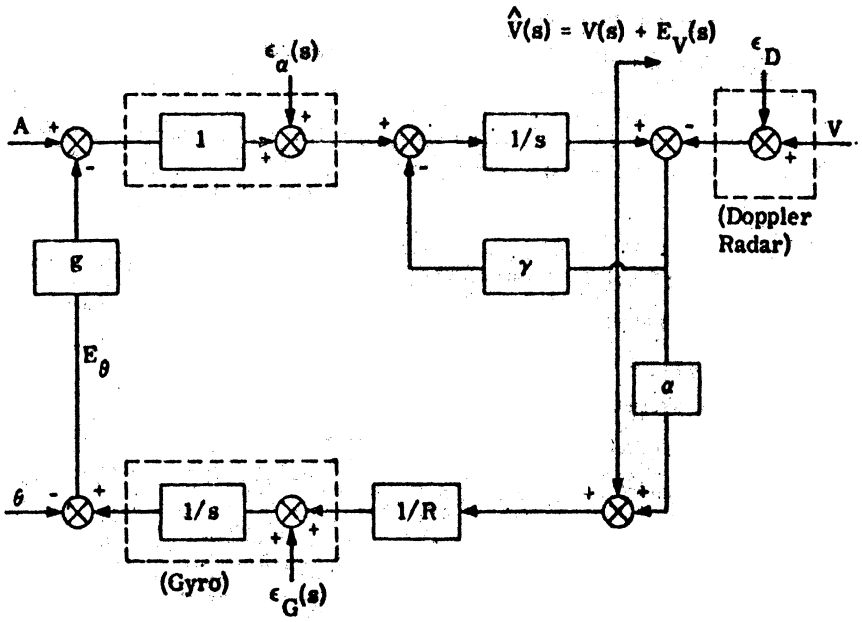

FIGURE 4. SECOND-ORDER D-I SYSTEM #1

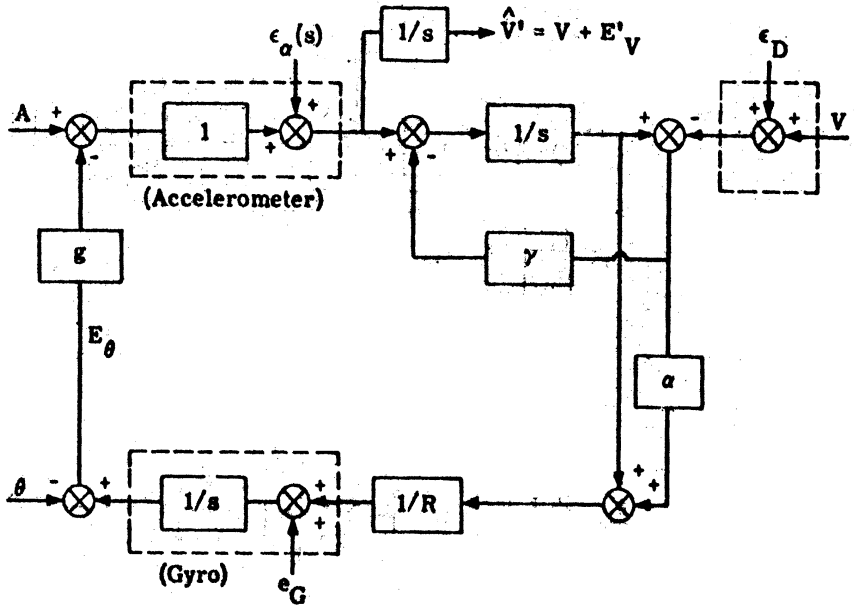

FIGURE 5. SECOND-ORDER D-I SYSTEM #2

separate integrator, thus yielding a new calculation of velocity. Let us denote the error in this calculation by $E'_V(s)$. It can be shown that this error is given by the expression

$$E'_V(s) = \frac{-g(1+\gamma/s)\epsilon_G(s) + \Omega^2(\alpha - \gamma/s)\epsilon_D(s) + (s+\gamma)\epsilon_\alpha(s)}{s^2 + \gamma s + (1+\alpha)\Omega^2} \tag{22}$$

Comparing Equations 21 and 22, we see that the high-frequency doppler noise affects the first output position through a gain $\approx \frac{1}{s}$, whereas it affects the second output through a gain $\approx \frac{1}{s^2}$. Thus the conclusion that second-order systems are necessarily plagued by this high-frequency noise is unmerited. Note that the second configuration has the disadvantage of an open-loop integrator, which may cause low-frequency drift problems. However, consider a third example given in Figure 6, where the Equation $E''_V(s)$ is given by

$$E''_V(s) = \frac{(s+\gamma)\epsilon_\alpha(s) - g(1+\gamma/s)\epsilon_G(s) + \Omega^2(\alpha - \gamma/s)\epsilon_D(s)}{s^2 + \gamma s + (1+\alpha)\Omega^2} \tag{23}$$

Clearly this is a second-order system whose sensitivity to high-frequency doppler noise is as good as that of the second example, and avoids open-loop integrator operation.

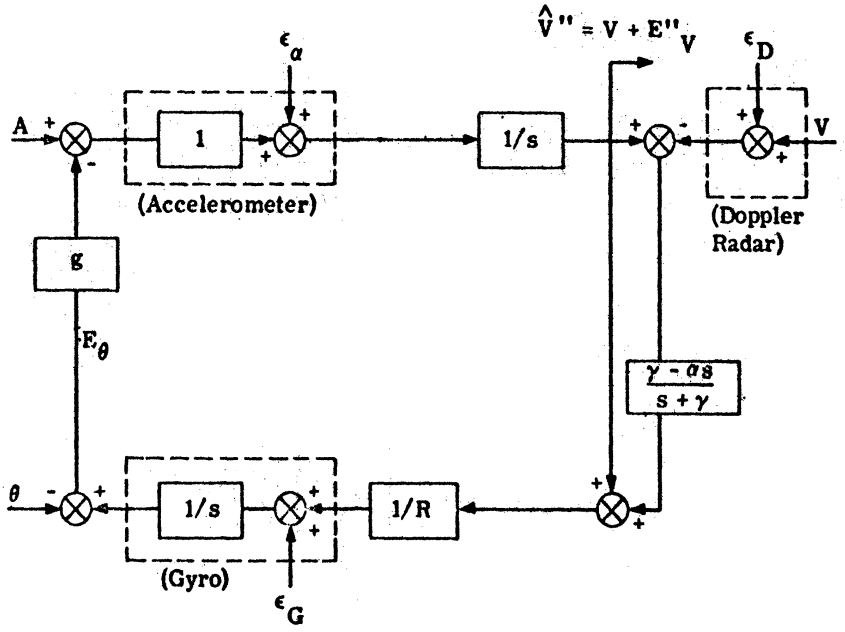

FIGURE 6. SECOND-ORDER D-I SYSTEM #3

By this time it is apparent that further examples can be concocted. For example, we may extract information from any of Figures 4, 5, and 6, directly ahead of the "division by R," and thus derive additional possibilities for second-order systems. Similar ambiguities can be found in inertial self-damped systems, where the system errors are functions of the particular damping and output positions.

In light of these examples, we can conclude that by failing to approach the system from a general view, one may reach false conclusions about system limitations.

2.3. UNCOUPLED HYBRIDIZATION

So far we have concentrated on D-I systems which are coupled by signal mixing within the system framework. This section will show that equivalent operations can be performed without disturbing the autonomies of the two component systems. Let us begin with the generalized system representation in Figure 7.

In Figure 7 there are two possible outputs — if we exclude the possibility of using an open-loop integrator and ignore direct readout from the doppler radar itself. Equations 24 and 25 describe the signals at these points.

$$\hat{V}_1(s) = V(s) + [s^2 + \Omega^2 Q(s)]^{-1} \left\{ s\epsilon_\alpha(s) - g\epsilon_G(s) - \Omega^2[1 - Q(s)]\epsilon_D(s) \right\} \tag{24}$$

$$\hat{V}_2(s) = V(s) + [s^2 + \Omega^2 Q(s)]^{-1} \left\{ sQ(s)\epsilon_\alpha(s) - gQ(s)\epsilon_G(s) + s^2[1 - Q(s)]\epsilon_D(s) \right\} \tag{25}$$

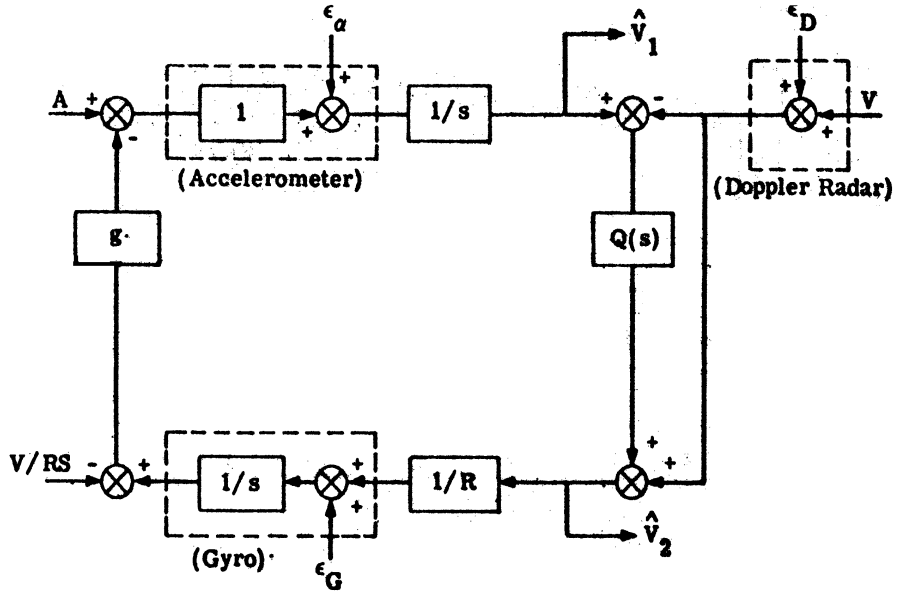

FIGURE 7. THE PRIMARY GENERAL D-I SYSTEM

We denote the errors in these signals as

$$E_{V_1}(s) = [s^2 + \Omega^2 Q(s)]^{-1}\left\{s\epsilon_\alpha(s) - g\epsilon_G(s) - \Omega^2[1 - Q(s)]\epsilon_D(s)\right\} \tag{26}$$

$$E_{V_2}(s) = [s^2 + \Omega^2 Q(s)]^{-1}\left\{sQ(s)\epsilon_\alpha(s) - gQ(s)\epsilon_G(s) + s^2[1 - Q(s)]\epsilon_D(s)\right\} \tag{27}$$

In comparing Equations 26 and 27, we note that apparently the first position would be much less sensitive to the high-frequency noise contributed by $\epsilon_D(s)$. However, the optimum Q(s) would not be the same for both velocity output positions; that is, optimizing Equations 26 and 27 will give different Q(s) forms for minimum error. Indeed it will shortly be shown that these respective minimum errors can be identical or not, according to how the optimization is conducted.

We shall use the term "uncoupled hybridization" to designate those D-I systems which function without intercoupling and whose hybridization is carried out by simple signal mixing in an output channel. This hybridization is represented in Figure 8.

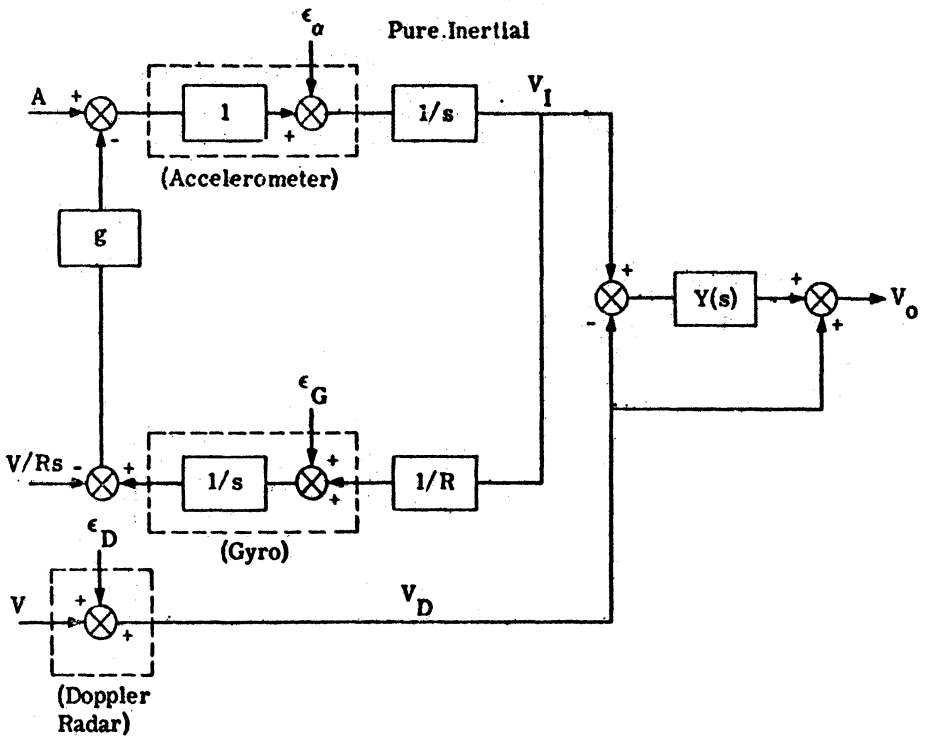

FIGURE 8. UNCOUPLED D-I SYSTEM

We shall use the designation $V_I(s)$ and $V_D(s)$ for the velocity output of a pure inertial and a pure doppler system. The system output is computed by mixing signals $V_I(s)$ and $V_D(s)$. It can be shown that the two signals are given by

$$V_I(s) = V(s) + \frac{s\epsilon_\alpha(s) - g\epsilon_G(s)}{s^2 + \Omega^2} \tag{28}$$

$$V_D(s) = V(s) + \epsilon_D(s) \tag{29}$$

Hence the output $V_o(s)$ can be computed to be

$$V_o(s) = V(s) + Y(s)\left[\frac{s\epsilon_\alpha(s) - g\epsilon_G(s)}{s^2 + \Omega^2}\right] + [1 - Y(s)]\,[\epsilon_D(s)] \tag{30}$$

We shall designate the error in V_o as $E_{V_o}(s)$, which is defined by

$$E_{V_o}(s) = Y(s)\left[\frac{s\epsilon_\alpha(s) - g\epsilon_G(s)}{s^2 + \Omega^2}\right] + 1 - [Y(s)\epsilon_D(s)] \tag{31}$$

To show that this open-loop hybridization produces the same signal as the closed-loop configuration in Figure 7, let us rewrite Equations 26 and 27 as follows:

$$E_{V_1}(s) = Y_1(s)\left[\frac{s\epsilon_\alpha(s) - g\epsilon_G(s)}{s^2 + \Omega^2}\right] + [1 - Y_1(s)]\epsilon_D(s) \tag{32}$$

where

$$Y_1(s) = \frac{s^2 + \Omega^2}{s^2 + \Omega^2 Q_1(s)} \tag{33}$$

and

$$E_{V_2}(s) = Y_2(s)\left[\frac{s\epsilon_\alpha(s) - g\epsilon_G(s)}{s^2 + \Omega^2}\right] + [1 - Y_2(s)]\epsilon_D(s) \tag{34}$$

where

$$Y_2(s) = \frac{(s^2 + \Omega^2)Q_2(s)}{s^2 + \Omega^2 Q_2(s)} \tag{35}$$

Because the filters and error sources appear in identical fashion in Equations 31, 32, and 34, the optimization process will lead to identical minimum errors. Although the optimum filters $Y_{o0}(s)$, $Y_{o1}(s)$, and

$Y_{o2}(s)$ will be identical, it is apparent from Equations 33 and 35 that the optimum filters $Q_{o1}(s)$, given by Equation 33, and $Q_{o2}(s)$, given by Equation 35, will differ. In fact, equating $Y_1(s)$ and $Y_2(s)$ shows that

$$Q_{o1}(s) = \frac{1}{\Omega^2}\left[\frac{s^2}{Q_{o2}(s)} + \Omega^2 - s^2\right] \tag{36}$$

We will now show that if the optimization process is performed from the intercoupled equations, the resulting minimum errors given by Equations 26 and 27 will differ. In Reference 1, a filter I(s) was defined as

$$I(s) = \frac{\Omega^2 Q(s)}{s^2 + \Omega^2 Q(s)} \tag{37}$$

By use of this filter, Equations 26 and 27 may be written

$$E_{V_1}(s) = I(s)[\epsilon_D(s)] + [1 - I(s)]\left[\frac{1}{s}\epsilon_\alpha(s) - \frac{g}{s^2}\epsilon_G(s) - \frac{\Omega^2}{s^2}\epsilon_D(s)\right] \tag{38}$$

$$E_{V_2}(s) = I(s)\left[\frac{s}{\Omega^2}\epsilon_\alpha(s) - \frac{g}{\Omega^2}\epsilon_G(s) - \frac{s^2}{\Omega^2}\epsilon_D(s)\right] + [1 - I(s)][\epsilon_D(s)] \tag{39}$$

If I(s) is optimized without constraints in Equations 38 and 39, the resulting minimum errors will be identical. (This is obvious, since we have merely rewritten Equations 26 and 27.) However, if we constrain the poles of I(s) to the left half of the complex s plane, the different forms of the noise sources in Equations 38 and 39 cause different minimum errors.

The crux of this argument is that the optimum filters $I_{o1}(s)$, given by Equation 32, and $I_{o2}(s)$, given by Equation 39, are optimized, in the constrained case, through a process which uses the separation of a polynomial into left-half and right-half plane parts. This operation is "nonlinear" and does not commute with the operation of substitution. To illustrate, let us perform a portion of the calculations. (Reference 1 gives detailed definitions of the following quantities.)

$$\psi_1(s)\psi_1(-s) = -\frac{1}{s^2}\left[g^2\Phi_G(s) - s^2\Phi_\alpha(s) + (s^2 + \Omega^2)^2\Phi_D(s)\right] \tag{40}$$

$$\psi_2(s)\psi_2(-s) = \frac{R^2}{g^2}\left[g^2\Phi_G(s) - s^2\Phi_\alpha(s) + (s^2 + \Omega^2)^2\Phi_D(s)\right] \tag{41}$$

hence

$$\psi_A(s)\psi_A(-s) = \frac{1}{s^2}\frac{R^2}{g^2}\psi_V(s)\psi_V(-s) \tag{42}$$

$$\psi_A(s) = \frac{1}{s}\frac{g}{R}\psi_V(s) = \frac{\Omega^2}{s}\psi_V(-s) \tag{43}$$

$$\psi_A(-s) = -\frac{1}{s}\frac{g}{R}\psi_V(-s) = -\frac{\Omega^2}{s}\psi_V(-s) \tag{44}$$

Now we define the combinations:

$$\Phi_1(s) = \Phi_{aaA}(s) + \Phi_{baA}(s) = -\frac{1}{s^2}\left[g^2\Phi_G(s) - s^2\Phi_\sigma(s) + (s^2+\Omega^2)\Phi_D(s)\right] \tag{45}$$

$$\Phi_2(s) = \Phi_{aaV}(s) + \Phi_{baV}(s) = \frac{1}{\Omega^2}(s^2+\Omega^2)\Phi_D(s) \tag{46}$$

By comparing Equations 45 and 46, we can see that

$$\Phi_1(s) = \Omega^2\Phi_2(s) - \left(\frac{g^2}{s^2R^2}\right)\psi_V(s)\psi_V(-s) = \Omega^2\Phi_2(s) - \frac{\Omega^4}{s^2}\psi_V(s)\psi_V(-s) \tag{47}$$

Now the optimum system forms are determined by the equations

$$I_{oV} = \frac{1}{\psi_V(-s)}\left[\frac{\Phi_2(s)}{\psi_V(-s)}\right]_{lhp} \tag{48}$$

$$I_{oA} = \frac{1}{\psi_A(s)}\left[\frac{\Phi_1(s)}{\psi_A(-s)}\right]_{lhp} \tag{49}$$

Substituting 43, 44, and 47 in 49, we have

$$I_{oA} = \frac{s}{\Omega^2\psi_V(s)}\left[\frac{\Omega^2\Phi_2(s) - \frac{\Omega^4}{s^2}\psi_V(s)\psi_V(-s)}{-\frac{\Omega^2}{s}\psi_V(-s)}\right]_{lhp} \tag{50}$$

$$I_{oA} = \frac{s}{\Omega^2\psi_V(s)}\left[\frac{\Omega^2}{s}\psi_V(s)\right]_{lhp} - \frac{s}{\Omega^2\psi_V(s)}\left[\frac{s\Phi_2(s)}{\psi_V(-s)}\right]_{lhp} \tag{51}$$

which reduces to

$$I_{oA}(s) = 1 - \frac{s}{\Omega^2 \psi(s)} \left[\frac{s\Phi_2(s)}{\psi_V(-s)} \right]_{lhp} \tag{52}$$

Hence if the condition of Equation 52 is to be consistent with the expression

$$I_{oA}(s) = 1 - \frac{s^2}{\Omega^2} I_{oV}(s) \tag{53}$$

then

$$s\left[\frac{\Phi_2(s)}{\psi_V(-s)} \right]_{lhp} = \left[\frac{s\Phi_2(s)}{\psi_V(-s)} \right]_{lhp} \tag{54}$$

which is clearly not always true.

3
SPECIFIC CONFIGURATION COMPARISONS

We turn our attention now to specific calculations of the available accuracy of several of the system configurations mentioned in Sections 2, 3, and 4. To do this, we will select a standard set of error sources (representing actual hardware reasonably well) and carry out optimization for the various configurations studied. The resultant maximum system performance can then be computed for each configuration.

3.1. PARAMETER DEFINITION OF ERROR-SOURCE POWER SPECTRA

The discussion of the power-spectra functions $\Phi_G(\omega)$, $\Phi_D(\omega)$, and $\Phi_\alpha(\omega)$ [2, 3, 4, 5] indicates that Φ_G will usually consist mainly of low-frequency content, and $\Phi_D(\omega)$ mainly of high-frequency content. Generally, $\Phi_\alpha(\omega)$ contains both low and high frequencies.

In the following example, the units used will be those of the mks system: $\Phi_G(\omega)$ is measured in (rad/sec)^2/unit bandwidth; $\Phi_\alpha(\omega)$ is measured in (m/sec^2)^2/unit bandwidth; and $\Phi_D(\omega)$ is measured in (m/sec)^2/unit bandwidth. The power spectra used in this calculation will be

$$\Phi_G(\omega) = \frac{0.15\pi\omega_G\sigma_G^2 \times 10^{-12}}{\omega_G^2 + \omega^2} \qquad (\text{rad/sec})^2/(\text{rad/sec}) \tag{55}$$

$$\Phi_D(\omega) = \pi\sigma_D^2 \qquad (m/sec)^2/(rad/sec) \qquad (56)$$

$$\Phi_\alpha(\omega) = \pi\sigma_\alpha^2 \times 10^{-8} \qquad (m/sec^2)^2/(rad/sec) \qquad (57)$$

In more familiar terminology, it can be shown that Equation 55 represents a typical gyro-drift-rate spectrum with a standard deviation of 0.1 σ_G degrees/hour and a correlation time of $1/\omega_G$ seconds. Equation 56 represents a velocity sensor with a white-noise error whose variance/unit bandwidth is σ_D^2 $(m/sec)^2$. Equation 57 represents an accelerometer with a variance/unit bandwidth of $\sigma_\alpha 10^{-4}$ $(m/sec)^2$, or roughly $\sigma_\alpha 10^{-5}$ g's.

In this as in other problems, the analysis is considerably simplified by introducing dimensionless parameters and variables. This particular calculation will be simplified by three such identifications:

$$\delta = \omega_G/\Omega \qquad \text{(dimensionless)} \qquad (58)$$

$$\Delta = 4.12\left(\delta\sigma_G^2/\sigma_D^2\right)^{1/6} \qquad \text{(dimensionless)} \qquad (59)$$

$$W = s/\Omega\Delta \qquad \text{(dimensionless)} \qquad (60)$$

At this point the definition of Equation 59 is far from obvious; suffice to say that when the quantity $\psi_V(s)\psi_V(-s)$ is expressed in terms of the variable W, it assumes an easily factorable form. The variable change of Equation 60 can, of course, be spelled out in more detail. If the complex variable W has the real and imaginary parts $W = \zeta + j\beta$, and the complex variable s has the real and imaginary form $s = \sigma + j\varphi$, then Equation 60 is equivalent to the two equations $\beta = \omega/\Omega\Delta$ and $\zeta = \sigma/\Omega\Delta$.

To provide a range of parameter consideration which realistically represents actual gyros, accelerometers, and velocity radars, the parameters will be assumed to be within the following limits:

$$0.1\Omega \leq \omega_G \leq \Omega \qquad (sec^2)^{-1} \qquad (61_1)$$

$$1 \leq \sigma_D \leq 3 \qquad (\sqrt{\pi}\ m/sec) \qquad (61_2)$$

$$0.1 \leq \sigma_\alpha \leq 0.3 \qquad (\sqrt{\pi}\ 10^{-4}\ m/sec^2) \qquad (61_3)$$

$$0.3 \leq \sigma_G \leq 10 \qquad \text{(tenths of degrees/hour)} \qquad (61_4)$$

From these limits it may be derived that

$$0.1 \leq \delta \leq 1 \qquad \text{(dimensionless)} \qquad (62_1)$$

$$0.1 \leq \Delta \leq 10 \qquad \text{(dimensionless)} \qquad (62_2)$$

3.2. PURE CROSSTRACK-VELOCITY OPTIMIZATION OF D-I SYSTEM

In this section, we shall optimize the configuration of Figure 2 with $\beta_o = 0^o$, that is, purely crosstrack-velocity sensing. In Reference 1, it is shown that the symbolic form for the optimum I(s) is given by

$$I_{oV}(s) = \frac{1}{\psi_V(s)}\left[\frac{\Phi_{aaV}(s/j) + \Phi_{baV}(s/j)}{\psi_V(-s)}\right]_{lhp} \qquad (63)$$

where

$$\Phi_{aaV}(s/j) + \Phi_{baV}(s/j) = (1 + s^2/\Omega^2)\Phi_D(s/j) \qquad (64)$$

and

$$\psi_V(s)\psi_V(-s) = (1/\Omega^4)\, g^2\Phi_G(s/j) - s^2\Phi_\alpha(s/j) + (s^2 + \Omega^2)^2\Phi_D(s/j) \qquad (65)$$

In the combination of spectra in Equation 65, $\Phi_\alpha(\omega)$ could almost be eliminated by inspection. At low frequencies, $\Phi_\alpha(\omega)$ is weighted with an ω^2, thus reducing its size in comparison with $\Phi_G(\omega)$, which is largest at low frequencies. At high frequencies, $\omega^2\Phi_\alpha(\omega)$ is compared with $\omega^4\Phi_D(\omega)$ and thus again is negligible. It should not be surprising if $\Phi_\alpha(\omega)$ plays a very minor role in determining $I_{oV}(s)$.

3.3. DERIVATION OF $I_{oV}(s)$

By means of Equations 63, 64, and 65, the symbolic specification of $I_{oV}(s)$ has been obtained; and through Equations 55, 56, and 57, it has been connected with the physical characteristics of the sensors. This cluster of information will now be reduced through a series of substitutions so that the final form of $I_{oV}(s)$ results. The work will begin with the calculation of $\psi_V(s)$, which proceeds in a straightforward manner. By substituting Equations 55, 56, and 57 into Equation 65, we find that

$$\psi_V(s)\psi_V(-s) = \frac{\pi}{\Omega^4}\left[\frac{0.15 g^2 \omega_G \sigma_G^2 \cdot 10^{-12}}{\omega_G^2 - s^2} - s^2\sigma_A^2 \cdot 10^{-8} + (s^2 + \Omega^2)^2\sigma_D^2\right] \qquad (66)$$

When the nondimensional parameter notations of Equations 58, 59, and 60 are introduced, this relationship is transformed thus:

$$\psi_V(W)\psi_V(-W) = \frac{\pi}{\Omega^4}\left[\frac{0.15K^2\delta_G\sigma_G^2\cdot 10^{-12}}{\omega_G^2 - \Omega^2\Delta^2W^2} + \Omega^2\Delta^2\sigma_A^2W^2\cdot 10^{-8} + \Omega^4(\Delta^2W^2+1)^2\sigma_D^2\right] \tag{67}$$

By removal of a common factor and straightforward manipulation, the relationship reduces to

$$\psi_V(W)\psi_V(-W) = \frac{\pi\sigma_D^2\Delta^6}{\delta^2 - \Delta^2W^2}(1 - W^6) \tag{68}$$

The fact that the six zeroes of Equation 68 lie exactly on the unit circle results from the frequency-scale transformations of Equations 59 and 60. It should be clear that these transformations were evolved from the development of Equation 68 in the s notation and are used here merely for simplicity. Equation 68 is easily factored into the following right-half and left-half plane parts:

$$\psi_V(W) = \frac{\sigma_D\Delta^3(W+1)(W^2+W+1)}{\Delta W + \delta}(\pi)^{1/2} \tag{69}$$

$$\psi_V(-W) = \frac{\sigma_D\Delta^3(W-1)(W^2-W+1)}{\Delta W - \delta}(\pi)^{1/2} \tag{70}$$

Equation 64 can also be expressed in terms of the W variable:

$$\Phi_{aaV}(W) + \Phi_{baV}(W) = (1 + \Delta^2W^2)\pi\sigma_D^2 \tag{71}$$

The optimum filter, $I_{oV}(W)$, follows directly from Equation 63:

$$I_{oV}(W) = \frac{(\pi)^{1/2}}{\psi_V(W)}\left[\frac{\sigma_D^2(1+\Delta^2W^2)(\Delta W - \delta)}{\sigma_D\Delta^3(W-1)(W^2-W+1)}\right]_{lhp} \tag{72}$$

The bracketed part of Equation 72 has no left-half plane poles. Now, however, the bracketed function approaches zero as W approaches infinity, a development which leads to the equivalent expanded form

$$I_{oV}(W) = \frac{(\pi)^{1/2}}{\psi_V(W)}\left[\sigma_D + \frac{K_2W^2 + K_1W + K_0}{(W-1)(W^2-W+1)}\right]_{lhp} \tag{73}$$

where σ_D is taken as the left-half plane part of this expression. Thus

$$I_{oV}(W) = \frac{(\pi)^{1/2}\sigma_D}{\psi_V(W)} \cdot \frac{\Delta W + \delta}{\Delta^3(W+1)(W^2+W+1)} \tag{74}$$

Equation 74 may be used to express this result in the original variable notation

$$I_{oV}(s) = \frac{\Omega^2(s+\Omega\delta)}{(s+\Omega\Delta)(s^2+\Omega\Delta s+\Omega^2\Delta^2)} \tag{75}$$

3.4. CALCULATION OF $\Phi_V(\omega)$

In this section, the optimum filter $I_{oV}(s)$ will be substituted back into the error equation which it minimizes. The resultant system-error power spectrum will be found and the standard deviation of this error calculated. To do this, recall that

$$\Phi_V(\omega) = [I_{oV}(j\omega) - 1][I_{oV}(-j\omega) - 1]\Phi_{aaV}(\omega) + [I_{oV}(-j\omega) - 1]I_{oV}(j\omega)\Phi_{abV}(\omega)$$

$$+ [I_{oV}(j\omega) - 1]I_{oV}(-j\omega)\Phi_{baV}(\omega) + I_{oV}(j\omega)I_{oV}(-j\omega)\Phi_{bbV}(\omega)$$

By rearrangement the equation becomes

$$\Phi_V(\omega) = I_{oV}(j\omega)I_{oV}(-j\omega)[\Phi_{aaV}(\omega) + \Phi_{abV}(\omega) + \Phi_{baV}(\omega) + \Phi_{bbV}(\omega)]$$

$$- I_{oV}(j\omega)[\Phi_{aaV}(\omega) + \Phi_{abV}(\omega)] - I_{oV}(-j\omega)[\Phi_{aaV}(\omega) + \Phi_{baV}(\omega)] + \Phi_{aaV}(\omega) \tag{76}$$

It is possible to attack Equation 76 directly with a barrage of substitutions for the various symbolic functions, but the process can be simplified considerably by noting the following factors. Equation 74 states that $I_{oV}(j\omega) = \sigma_D/\psi_V(j\omega)$ and $I_{oV}(-j\omega) = \sigma_D/\psi_V(-j\omega)$. Furthermore, the term inside the first parenthesis of Equation 76 is by definition $\psi_V(j\omega)\psi_V(-j\omega)$. In addition we note that $\Phi_{aaV}(\omega) = \sigma_D^2$ and $\Phi_{abV}(\omega) = \Phi_{baV}(\omega)$. With these facts in mind, we can reduce Equation 76 to

$$\Phi_V(\omega) = \pi\sigma_D^2\left\{2 - \left(1 + \frac{s^2}{\Omega^2}\right)[I_{oV}(j\omega) + I_{oV}(-j\omega)]\right\} \tag{77}$$

The following calculations, like those preceding, are most easily handled with the terminology of the W variable. If Equation 74 is used, then Equation 77 can be shown to reduce to

$$\Phi_V(W) = 2\pi\sigma_D^2\left[\frac{W^4\Omega^2(2\Delta^2 + 1 - 2\delta\Delta) + W^2\Omega^4(2\delta\Delta + \delta\Delta^3 - 2\Delta^2) + \Omega^6\Delta^3(\Delta^3 - \delta)}{W^6 + \Omega^6\Delta^6}\right] \tag{78}$$

3.5. CALCULATION OF σ_V^2

The square of the standard deviation of the system velocity-measurement error can be obtained by integrating Equation 78 from zero to infinity. The integration is facilitated by making the change of variable $\beta = \frac{\omega}{\Omega\Delta}$; hence $d\omega = \Omega\Delta d\beta$. In terms of the β variable, the integral becomes

$$\sigma_V^2 = 2\sigma_D^2\int_0^\infty \frac{(2 + \Delta^{-2} - 2\delta\Delta^{-1})\beta^4 + (2\delta\Delta^{-3} + \delta\Delta^{-1} - 2\Delta^{-2})\beta^2 + (1 - \delta\Delta^{-3})}{1 + \beta^6}\Omega\Delta\, d\beta \tag{79}$$

three standard definite integrals will be useful:

$$\int_0^\infty \frac{dx}{1 + x^6} = \frac{\pi}{3} \tag{80$_1$}$$

$$\int_0^\infty \frac{x^2 dx}{1 + x^6} = \frac{\pi}{6} \tag{80$_2$}$$

$$\int_0^\infty \frac{x^4 dx}{1 + x^6} = \frac{\pi}{3} \tag{80$_3$}$$

By dividing Equation 79 into three integrals and applying the appropriate integral given in Equations 80_1, 80_2, and 80_3, the evaluation of σ_V^2 becomes

$$\sigma_V^2 = 2\Omega\Delta\sigma_D^2\left[(2 + \Delta^{-2} - 2\delta\Delta^{-1})\frac{\pi}{3} + (2\delta\Delta^{-3} + \delta\Delta^{-1} - 2\Delta^{-2})\frac{\pi}{6} + (1 - \delta\Delta^{-3})\frac{\pi}{3}\right] \tag{81}$$

By combining terms, Equation 81 may be simplified to the expression

$$\sigma_V^2 = 2\Omega\pi\Delta\sigma_D^2\left[1 + \frac{\delta}{6\Delta}\left(\frac{2}{\Delta^2} - 5\right)\right] \tag{82}$$

Since $\delta < 1$ and $\Delta > 1$, a good first-order approximation of this result would be

$$\sigma_V^2 = 2\Omega\pi\Delta\sigma_D^2 \tag{83}$$

If the original definition of Δ (Equation 59) is used,

$$\sigma_V^2 = 8.24\pi\Omega\sigma_D^2\left(\delta\sigma_G^2/\sigma_D^2\right)^{1/6} \qquad (84_1)$$

A graph of Equation 84_1 and a discussion of this result are provided in Volume II.

The sequel includes the computation and comparison of standard deviations for many other configurations. The variety to be encountered makes mandatory the adoption of a standard subscript notation which conveys the identification of error being described. Since all errors to be minimized are velocity-measurement errors, we shall omit "V" as a subscript. The notation to be used is $\sigma^2_{(\ ),(\ ),(\ )}$.

The first group will use either DI or I to indicate doppler-inertial or inertial system, respectively. The second group will use NE or E to indicate nonexact (dependent upon the motion itself) or exact (independent of motion), respectively. The third group will indicate the amount of filter delay time allowed: 0 - no delay; ∞ - infinite delay; T - T seconds delay. To illustrate, Equation 84_1 becomes

$$\sigma^2_{DI,\,E,\,0} = 8.24\pi\Omega\sigma_D^2\left(\delta\sigma_G^2/\sigma_D^2\right)^{1/6} \qquad (84_2)$$

4
DELAYED-DATA OPERATION OF A D-I SYSTEM

4.1. INTRODUCTION

In this section, we shall consider the feasibility of using a delayed-data motion-sensing system for motion compensation. The operative rationale is that a system may be able to derive compensating signals of considerably improved fidelity for the high-resolution radar system if this derivation need not be instantaneous. This means, however, that the radar information must also be delayed by an equal time interval; hence it is more than merely possible that the increased complexity would far overshadow any gain in system performance.

In addition, we can derive an increase in precision, basing our design on a knowledge of vehicle perturbations.

We begin this discussion by considering the simplest of the many possible block diagrams. Figure 9 depicts a D-I system whose output is fed to a linear interpolator. The ideal interpolator would yield as an

output the true velocity at a time T seconds ago. Hence, we may judge our interpolator's performance by examining the difference between its output and the ideal output. This difference has been designated $E_o(s)$. $E_o(s)$ is given by

$$E_o(s) = E_V H(s) + [H(s) - e^{-sT}] V_T(s) \tag{85}$$

The system of Figure 9 is identical in form to that of Figure 10, where X = the signal, n = the noise, and $E_o(s)$ takes the form

$$E_o(s) = n(s)H(s) + (H - e^{-sT})X(s) \tag{86}$$

Thus, comparing Equations 85 and 86, we see that $E_V(t) = n(t)$ = the noise input to the system; and $X(t) = V(t)$ = the signal input to the system. In the actual case, E_V is the error in the system's measurement of V_T and hence (as has been discussed in Section I) is a function of the various mixing configurations chosen.

To illustrate the techniques involved in this problem, let us make a simple introductory calculation.

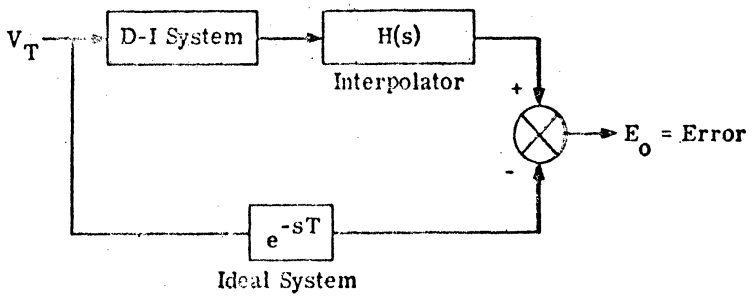

FIGURE 9. DELAYED-DATA D-I SYSTEM

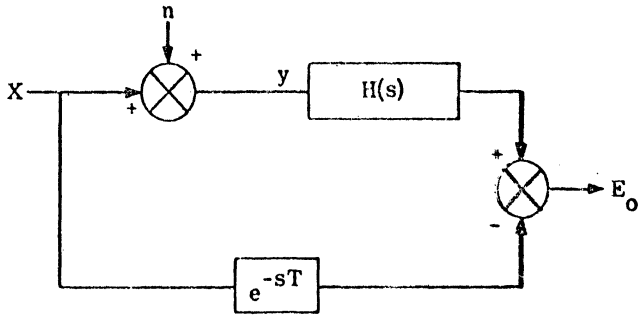

FIGURE 10. CONVENTIONAL FILTER PROBLEM

4.2 ILLUSTRATIVE CALCULATION

Let us find by means of the Wiener filter theory the optimum realizable H(s), for estimation of X(t - T). Our optimizing criteria is an integrated squared error. We assume for this example that the signal and noise are independent, with respective power spectra given by

$$\Phi_{XX}(\omega) = \frac{1}{1 + \omega^2} \tag{87}$$

$$\Phi_{nn}(\omega) = \frac{\omega^2}{1 + \omega^2} \tag{88}$$

Hence

$$\Phi(\omega) = \Phi_{XX}(\omega) + \Phi_{nn}(\omega) = 1 \tag{89}$$

at all ω. We assume here that $\Phi(\omega)$ is factorable into exclusive left-half and right-half parts and hence is expressible as

$$\Phi(\omega) = \Phi^{+}(\omega)\Phi^{-}(\omega) \tag{90}$$

where $\Phi^{+}(\omega)$ contains all its poles and zeros of $\Phi(s/j)$ in lhp

$\Phi^{-}(\omega)$ contains all its poles and zeros of $\Phi(s/j)$ in rhp

$\Phi(\omega)$ is factorable in this sense if

$$\int_{-\infty}^{\infty} \frac{\log \Phi(\omega)}{1 + \omega^2} < \infty \tag{91}$$

Following standard techniques for optimization, we arrive at the conditions

$$\left[\Phi^{+}(\omega)H(\omega) - \frac{P(\omega)\Phi_{X(X+n)}(\omega)}{\Phi^{-}(\omega)}\right] = 0 \tag{92}$$

$$H(\omega) = \frac{1}{\Phi^{+}(\omega)} \cdot F^{-1}\left\{\left[\frac{\Phi_{XX}(\omega)\Gamma(\omega)}{\Phi^{-}(\omega)}\right] u(t)\right\} \tag{93}$$

where F = the Fourier transform

F^{-1} = the inverse transform

u(t) = unit step function

In this example $P(\omega)$ · ideal filter = $e^{-j\omega T}$ (94)

$$\Phi^{+}(\omega) = 1 \tag{95$_1$}$$

$$\Phi^{-}(\omega) = 1 \tag{95$_2$}$$

For independent signal and noise we have

$$\Phi_{X(X+n)}(\omega) = \Phi_{XX}(\omega)$$

and

$$\frac{\Phi_{XX}(\omega)P(\omega)}{\Phi^{-}(\omega)} = \frac{e^{-j\omega T}}{1+\omega^2} \tag{96}$$

From the Fourier transformation calculus, it can be shown that

$$L(t) = F^{-1}\left(\frac{e^{-j\omega T}}{1+\omega^2}\right) = e^{-|\tau - T|} \tag{97}$$

which is shown in Figure 11. L(t)u(t) is shown in Figure 12.

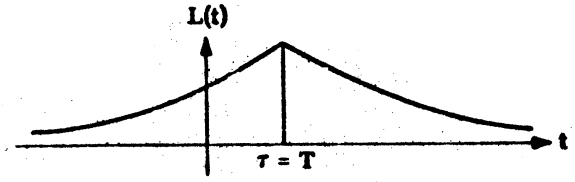

FIGURE 11. NONREALIZABLE WEIGHTING FUNCTION

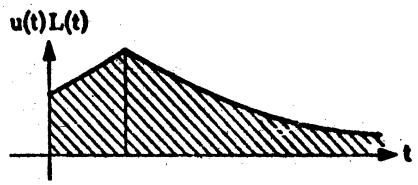

FIGURE 12. REALIZABLE WEIGHTING FUNCTION

The impulse response of the optimum realizable filter associated with Equation 92 is given by

$$h(t) = e^{-|t-T|}u(t) \tag{98}$$

The transfer function H(jω) of this system is determined by

$$H(j\omega) = \int_0^\infty h(t)\, e^{-j\omega T}\, dt \tag{99}$$

which in light of Equation 98 is

$$H(j\omega) = \int_0^\infty e^{-|t-T|}\, e^{-j\omega T}\, dt \tag{100}$$

Evaluation of this integral results in

$$H(j\omega) = \frac{e^{-j\omega T} - e^{-T}}{(1 - j\omega)} + \frac{e^{-j\omega T}}{(1 + j\omega)} \tag{101}$$

Equation 101 represents a stable transfer function since the singularity at jω = 1 is removable. This is evident if we expand the numerator in a Taylor series as follows:

$$e^{-j\omega T} - e^{-T} = \left[1 - j\omega T + \frac{(j\omega T)^2}{2!} - \frac{(j\omega T)^3}{3!} + \frac{(j\omega T)^4}{4!} \cdots\right] - \left(1 - T + \frac{T^2}{2!} - \frac{T^3}{3!} + \frac{T^4}{4!} \cdots\right) \tag{102}$$

or

$$e^{-j\omega T} - e^{-T} = T(1 - j\omega) - \frac{T^2}{2!}[1 - (j\omega)^2] + \frac{T^3}{3!}[1 - (j\omega)^3] + \cdots \tag{103}$$

Therefore

$$\left(\frac{e^{-j\omega T} - e^{-T}}{1 - j\omega}\right) = T - \frac{T^2}{2!}(1 + j\omega) + \frac{T^3}{3!}[1 + j\omega + (j\omega)^2] + \frac{T^4}{4!}(1 + j\omega)[1 + (j\omega)^2] + \cdots \tag{104}$$

Let jω = s. Then $\frac{e^{-sT} - e^{-T}}{1 - s}$ is analytic in the whole complex plane, and therefore can be represented by a power series about s = 0. If we let

$$\frac{e^{-sT} - e^{-T}}{1 - s} = F(s) \tag{105}$$

then by expansion about the origin

$$F(s) = \sum_{0}^{\infty} a_n s^n \tag{106}$$

where

$$a_n = \frac{F^{(n)}(s)}{n!} = \frac{1}{n!}\left[\frac{d^n F(s)}{ds^n}\right] \tag{107}$$

The optimum realizable filter has a transfer function that can be put in the following form

$$H(s) = \frac{e^{-j\omega T}}{s+1} + \sum_{n=0}^{\infty} a_n s^n \tag{108}$$

The minimum realizable standard deviation can be calculated from the expression

$$\sigma_{\epsilon r}^{\ 2} = \sigma_{\epsilon\infty}^{\ 2} + \int_{-\infty}^{0} \left| L^2(t) \right| dt \tag{109}$$

where $\sigma_{\epsilon r}^{\ 2}$ = minimum realizable standard deviation

$\sigma_{\epsilon\infty}^{\ 2}$ = minimum nonrealizable standard deviation

Using Equation 97,

$$\int_{-\infty}^{0} \left| L(t) \right|^2 dt = \frac{e^{-2T}}{2} \tag{110}$$

Also, $\sigma_{\epsilon\infty}^{\ 2}$ is given by

$$\sigma_{\epsilon\infty}^{\ 2} = \frac{1}{2\pi} \int_{-\infty}^{\infty} \left| P \right|^2 \left[\frac{\Phi_{XX}(\omega)\Phi_{nn}(\omega)}{\Phi_{XX}(\omega) + \Phi_{nn}(\omega)}\right] d\omega \tag{111}$$

In our example $\left|P\right|^2 = \left|e^{-j\omega T}\right|^2 = 1$: hence we have

$$\sigma_{\epsilon\infty}^{\ 2} = \frac{1}{2\pi} \int_{-\infty}^{\infty} \frac{\omega^2}{(1+\omega^2)^2} d\omega \tag{112}$$

Evaluating this integral and using Equation 110 results in

$$\sigma_{\epsilon r}^2(T) = \frac{e^{-2T}}{2} + (1 + \pi/4) \tag{113}$$

Equation 113 has a classic form for this type of problem. $\sigma_{\epsilon r}^2(T)$ is composed of a constant, $(1 + \pi/4)$, representing the minimum σ^2 for filters with poles in either half of the complex plane, and a contribution due to the realizability constraining $e^{-2T}/2$. Since T is the amount of delay in the filter, Equation 113 shows that the increase in accuracy, that is, decrease in $\sigma_{\epsilon r}^2(T)$, is asymptotic with T, as anticipated.

Now returning to the V-I system case, where we have from previous work:

$$E_V(s) = (I(s) - 1)\,\epsilon_{aV}(s) + I(s)\,\epsilon_{bV}(s) \tag{14}$$

From Equation 85 it can be concluded that:

$$\Phi_{oo}(\omega) = H(j\omega)\,H(-j\omega)\,\Phi_{EV}(\omega) + \left(H(j\omega) - e^{-j\omega T}\right)\left(H(-j\omega) - e^{+j\omega T}\right)\Phi_{V_T}(\omega) \tag{115}$$

Obtaining $\Phi_{EV}(\omega)$ from Equation 114 and substituting in Equation 115 results in

$$\Phi_{oo}(\omega) = H(j\omega)H(-j\omega)\Big\{[I(j\omega) - 1][I(-j\omega) - 1]\Phi_{aaV}(\omega) + [I(-j\omega) - 1]I(j\omega)\Phi_{abV}(\omega)$$

$$+ [I(j\omega) - 1]\,I(-j\omega)\Phi_{baV}(\omega) + I(j\omega)I(-j\omega)\Phi_{bbV}(\omega)\Big\}$$

$$+ [H(j\omega) - e^{-j\omega T}][H(-j\omega) - e^{+j\omega T}]\,\Phi_{V_T}(\omega) \tag{116}$$

Equation 116 represents the power spectrum of the output error of the interpolation of Figure 9. The rms values of this error are given by

$$\sigma_o^2 = \frac{1}{2\pi}\int_{-\infty}^{\infty}\Phi_{oo}(\omega)\,d\omega \tag{117}$$

To keep calculations to a minimum, we assume that I(s) has been chosen in advance possibly to minimize $E_V(s)$ itself. The job that remains, as in the foregoing example, is the selection of optimum H(s).

4.2.1. NONREALIZABLE CASE. If we do not require physical realizability for H(s), we can use the techniques of the previous work—which lead to the result

$$H(\omega) = \frac{\Phi_{V_T}(\omega)}{\Phi_{V_T}(\omega) + \Phi_{EV}(\omega)}\,e^{-j\omega T} \tag{118}$$

where $\Phi_{V_T}(\omega)$ = power spectrum of the signal and $\Phi_{EV}(\omega)$ = power spectra of noise (independent of signal).

4.2.2. REALIZABLE CASE. Following the illustrative calculation

$$\Phi_V(\omega) = \Phi_{V_T}(\omega) + \Phi_{EV}(\omega) \tag{119}$$

Again we have assumed that $\Phi_V(\omega)$ is to be factorized into $\Phi_V^+(\omega)$ and $\Phi_V^-(\omega)$, that is,

$$\Phi_V(\omega) = \Phi_V^+(\omega)\,\Phi_V^-(\omega) \tag{120}$$

where $\Phi_V^+(\omega)$ contains left-half plane poles only, and $\Phi_V^-(\omega)$ contains right-half plane poles only. The optimum, $H(j\omega)$, then takes the form

$$H(j\omega) = \frac{1}{\Phi_V^+(\omega)} F\left[F^{-1}\left(\frac{\Phi_{V_T} e^{-j\omega T}}{\Phi_V^-(\omega)}\right) u(T)\right] \tag{121}$$

where u(t) is the unit step function. As before, we use the notations

$$L(t) = F^{-1}\left[\frac{\Phi_{V_T}(\omega)e^{-j\omega T}}{\Phi_V^-(\omega)}\right] \tag{122}$$

$$\sigma_{\epsilon r}^2 = \sigma_{\epsilon\infty}^2 + \int_{-\infty}^{0} |L(t)|^2 dt \tag{123}$$

or

$$\sigma_{\epsilon r}^2(t) = \frac{1}{2\pi}\int_{-\infty}^{\infty}\left[\frac{\Phi_{V_T}(\omega)\Phi_{EV}(\omega)}{\Phi_{V_T}(\omega) + \Phi_{EV}(\omega)}\right] d\omega + \int_{-\infty}^{0} |L^2(\tau, T)| d\tau \tag{124}$$

The first term in Equation 124 is a constant independent of T; the second part depends, of course, on T. We will assume the D-I system to be affected by a random gyro drift rate, $\Phi_G(\omega)$, a random accelerometer noise, $\Phi_\alpha(\omega)$, and a random doppler error, $\Phi_D(\omega)$. To see how $\sigma^2(T)$ varies with T, we take the realistic error-source power spectra defined in Equations 55–62 of Section 3.1. In Section 3.3, we have shown that the optimum I(s) form for these error sources is

$$I_{oV}(s) = \frac{\Omega^2(s + \Omega\delta)}{(s + \Omega\Delta)(s^2 + \Omega\Delta s + \Omega^2\Delta^2)} \tag{75}$$

and Section 3.4 shows the minimum $\Phi_{EV}(\omega)$ to be

$$\Phi_{EV}(\omega) = 2\pi\sigma_D^2\left[\frac{\omega^2\Omega^2(2\Delta^2+1-2\delta\Delta)+\omega^2\Omega^4(2\delta\Delta+\delta\Delta^3-2\Delta^2)+\Omega^6\Delta^3(\Delta^3-\delta)}{\omega^6+\Omega^6\Delta^6}\right] \quad (78)$$

Finally we will assume velocity-perturbation power spectrum to be of the form

$$\Phi_{V_T}(\omega) = \frac{K_v^2}{\omega_v^2+\omega^2} \quad (125)$$

Adding Equations 78 and 125 and setting $\omega_v = 1$, we find that

$$\Phi_V^+(\omega)\Phi_V^-(\omega) = 2\pi\sigma_D^2\left[\frac{\omega^4\Omega^2(2\Delta^2+1-2\delta\Delta)+\omega^2\Omega^4(2\delta\Delta+\delta\Delta^3-2\Delta^2)+\Omega^6\Delta^3(\Delta^3-\delta)}{\omega^6+\Omega^6\Delta^6}\right]+\left[\frac{K_v^2}{\omega^2+1}\right] \quad (126)$$

The combined numerator, $N(\omega)$, of this expression has the form

$$N(\omega) = A_1\omega^6 + B_1\omega^4 + C_1\omega^2 + D_1 \quad (127)$$

where

$$A_1 = 2\pi\Omega^2\sigma_D^2(2\Delta^2+1-2\delta\Delta)+K_v^2 \approx K_v^2 \quad (128)$$

$$B_1 = 2\pi\sigma_D^2\Omega^4(2\delta\Delta+\delta\Delta^3-2\Delta^2)+2\pi\sigma_D^2\Omega^2(2\Delta^2+1-2\delta\Delta) \quad (129)$$

$$C_1 = 2\pi\sigma_D^2\Omega^6\Delta^3(\Delta^3-\delta)+2\pi\sigma_D^2\Omega^4(2\delta\Delta+\delta^3-2\Delta^2) \quad (130)$$

$$D_1 = \Omega^6\left[K_V^2\Delta^6+2\pi\sigma_D^2\Delta^3(\Delta^3-\delta)\right] \quad (131)$$

hence

$$\Phi_V^+(\omega)\Phi_V^-(\omega) = \frac{A\omega^6 + B\omega^4 + C\omega^2 + D}{(\omega^6 + \Omega^6\Delta^6)(\omega^2 + 1)} \tag{132}$$

For ω large,

$$N(\omega) = \omega^6\left(A_1 + \frac{B_1}{\omega^2} + \frac{C_1}{\omega^4} + \frac{D_1}{\omega^6}\right) \tag{133}$$

For ω small,

$$N(\omega) = \omega^2\left(A_1\omega^4 + B_1\omega^2 + C_1\right) + D_1 \tag{134}$$

At high and low frequency, the B_1 and C_1 terms can be neglected. By comparing the relative sizes of A, B, C, and D, we can conclude that B_1 and C_1 are negligible at all frequencies.

Equation 132 reduces to

$$\Phi_V^+(\omega)\Phi_V^-(\omega) = \frac{(A_1)\left(\omega^6 + \frac{D_1}{A_1}\right)}{(\omega^6 + \Omega^6\Delta^6)(\omega^2 + 1)} \tag{135}$$

Now we define

$$\gamma^6 = \Omega^6\Delta^6 \tag{136_1}$$

$$\beta^6 = D_1/A_1 \tag{136_2}$$

For the range of parameters selected for this calculation (Equations 55-62), β^6 can be approximated by

$$\beta^6 \cong \Omega^6\Delta^6 + \frac{2\pi\sigma_D^2\Omega^6\Delta^6}{K_v^2} \tag{136_3}$$

and therefore Equation 135 becomes

$$\Phi_V^+(\omega)\Phi_V^-(\omega) = A_1\left[\frac{\omega^6 + \beta^6}{(\omega^6 + \gamma^6)(\omega^2 + 1)}\right] \tag{137}$$

Now Equation 137 can be factorized as follows:

$$\omega^6 + \beta^6 = (\omega - \beta_1)(\omega - \beta_2)(\omega - \beta_3)(\omega \beta_4)(\omega - \beta_5)(\omega - \beta_6) \tag{138}$$

where

$$\beta_1 = \beta(\cos 30^\circ + j \sin 30^\circ) = \beta\left(\frac{\sqrt{3}}{2} + j\frac{1}{2}\right) \tag{139}$$

$$\beta_2 = j\beta \tag{140}$$

$$\beta_3 = \beta\left(\frac{\sqrt{3}}{2} + j\frac{1}{2}\right) \tag{141}$$

$$\beta_4 = \beta\left(\frac{\sqrt{3}}{2} - j\frac{1}{2}\right) \tag{142}$$

$$\beta_5 = -j\beta \tag{143}$$

$$\beta_6 = \beta\left(\frac{\sqrt{3}}{2} - j\frac{1}{2}\right) \tag{144}$$

And

$$\omega^6 + \gamma^6 = (\omega - \gamma_1)(\omega - \gamma_2)(\omega - \gamma_3)(\omega - \gamma_4)(\omega - \gamma_5)(\omega - \gamma_6) \tag{145}$$

where the roots γ_1 through γ_6 correspond to β_1 through β_6, respectively, except for the appropriate magnitude factor. Finally,

$$\omega^2 + 1 = (\omega + j)(\omega - j) \tag{146}$$

In terms of this notation, Equation 137 can be separated into

$$\Phi_V^+\left(\frac{s}{j}\right) = K_v \frac{(s - j\beta_1)(s - j\beta_2)(s - j\beta_3)}{(s - j\gamma_1)(s - j\gamma_2)(s - j\beta_3)(s + 1)} \tag{147}$$

and

$$\Phi_V^-\left(\frac{s}{j}\right) = K_v \frac{(s - j\beta_4)(s - j\beta_5)(s - j\beta_6)}{(s - j\gamma_4)(s - j\gamma_5)(s - j\gamma_6)(s - 1)} \tag{148}$$

Now, to get L(t) from Equation 122, we need

$$\left(\frac{\Phi_{V_T}\left(\frac{s}{j}\right)e^{-sT}}{\Phi_V^-\left(\frac{s}{j}\right)}\right) = \frac{K_v(s - j\gamma_4)(s - j\gamma_5)(s - j\gamma_6)e^{-sT}}{(s + 1)(s - j\beta_4)(s - j\beta_5)(s - j\beta_6)} \tag{149}$$

Equation 149 can be put in partial fraction form:

$$\left[\frac{\Phi_{V_T}\left(\frac{s}{j}\right)e^{-sT}}{\Phi_V^-\left(\frac{s}{j}\right)}\right] = \left[\frac{A}{s + 1} + \frac{B}{s - j\beta_4} + \frac{C}{s - j\beta_5} + \frac{D}{(s - j\beta_6)}\right]e^{-sT} \tag{150}$$

If we let

$$\Lambda^6 = 1 + \frac{2\pi\sigma_D^2}{K_v^2} \tag{151}$$

then $\beta = \Omega\Delta\Lambda$, and the constants A, B, C, and D are given by the approximate expressions

$$A \simeq K \tag{152}$$

$$B \simeq \frac{1}{2}\Delta\Omega K_v(\Lambda - 1)(\sqrt{2} - j\sqrt{3}) \tag{153}$$

$$C \simeq \frac{1}{4}K_v\Omega\Delta(1 - \Lambda)(1 - \Lambda)\left(1 + \frac{1}{\Lambda}\right)^2 \tag{154}$$

$$D \simeq \frac{1}{2}\Omega K_v\Delta(\Lambda - 1)(\sqrt{2} + j\sqrt{3}) \tag{155}$$

Since Ω is of the order 10^{-3}, the dominant residue in Equation 150 is A. The function of Equation 150 has its poles as shown in Figure 13. We can find L(t) by contour integration, the results of which are

$$L(t) = F^{-1}\left[\frac{\Phi_{V_T}\left(\frac{s}{j}\right)e^{-sT}}{\Phi_V^+\left(\frac{s}{j}\right)}\right] = Ae^{-(t-T)} \qquad t > T$$

$$= Be^{j\beta_4(t-T)} + Ce^{j\beta_5(t-T)} + De^{j\beta_6(t-T)} \qquad t < T \tag{156}$$

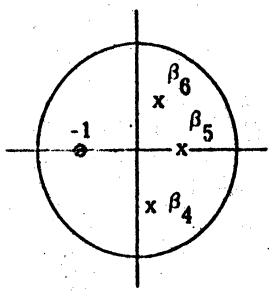

FIGURE 13. POLE-ZERO PLOT

Applying Equation 95 (restated here),

$$H(\omega) = \frac{1}{\Phi_V^+(\omega)} F\left[F^{-1}\left(\frac{\Phi_{V_T}\left(\frac{s}{j}\right) e^{-st}}{\Phi_V^+\left(\frac{s}{j}\right)} \right) u(t) \right] \tag{95}$$

We arrive at

$$H(s) = \frac{1}{K_v}\left[\frac{(s - j\gamma_1)(s - j\gamma_2)(s - j\gamma_3)(s + 1)}{(s - j\beta_1)(s - j\beta_2)(s - j\beta_3)} \right]$$

$$x\left[\frac{Ae^{-sT}}{s+1} + B\left(\frac{e^{st} - e^{j\beta_4 T}}{j\beta_4 - s} \right) + C\left(\frac{e^{st} - e^{j\beta_5 T}}{j\beta_5 - s} \right) + D\left(\frac{e^{st} - e^{j\beta_6 T}}{j\beta_6 - s} \right) \right] \tag{157}$$

Equation 157 reduces to

$$H(s) = \frac{1}{K_v} \frac{(s+1)\left[s^3 - j(\gamma_1 + \gamma_2 + \gamma_3)s^2 - (\gamma_1\gamma_2 + \gamma_2\gamma_3 + \gamma_1\gamma_3)s + j\gamma_1\gamma_2\gamma_3 \right]}{\left[s^3 - j(\beta_1 + \beta_2 + \beta_3)s^2 - (\beta_1\beta_2 + \beta_2\beta_3 + \beta_1\beta_3)s + j\beta_1\beta_2\beta_3 \right]}$$

$$x\left[\frac{Ae^{-sT}}{s+1} + B\left(\frac{e^{st} - e^{j\beta_4 T}}{j\beta_6 - s} \right) + C\left(\frac{e^{st} - e^{-j\beta_5 T}}{j\beta_5 - s} \right) + D\left(\frac{e^{st} - e^{j\beta_6 T}}{j\beta_6 - s} \right) \right] \tag{158}$$

Since the B, C, and D terms are small compared to the term A, a good approximation for H(s) is

$$H(s) = \frac{\left[s^3 + (\Omega\Delta)(1+\sqrt{2})s^2 + (\Omega\Delta)^2(1+\sqrt{2})s + \frac{5}{4}(\Omega\Delta)^3\right]e^{-sT}}{s^3 + \left[(\Omega\Delta)\left(1+\frac{2\pi\sigma_D^2}{K_v^2}\right)^{1/\sigma}(1+\sqrt{2})\right]s^2 + \left[(\Omega\Delta)^2\left(1+\frac{2\pi\sigma_D^2}{K_v^2}\right)^{1/3}(1+\sqrt{2})\right]s + \frac{5}{4}(\Omega\Delta)^3\left(1+\frac{2\pi\sigma_D^2}{K_v^2}\right)^{1/2}} \tag{159}$$

where the β's and γ's have been eliminated. Finally, we apply Equation 124 to get $\sigma_{\epsilon r}^2(t)$. As stated before, the first part of this equation is that due to the nonrealizable filter and the second part is due to the realizability constraint.

4.3. CALCULATION OF σ^2 FOR THE NONREALIZABLE CASE

Now, by using Equations 78, 125, and 132 we find that

$$\frac{\Phi_{V_T}(\omega)\Phi_{EV}(\omega)}{\Phi_{V_T}(\omega)+\Phi_{EV}(\omega)} = \left(2\pi\sigma_D^2\right)K_v^2\left[\frac{\omega^4\Omega^2(2\Delta^2+1-2\delta\Delta)+\omega^2\Omega^4(2\delta\Delta+\delta\Delta^3-2\Delta)^2+\Omega^5\Delta^3(\Delta^3-\delta)}{A_1\omega^6+B_1\omega^4+C_1\omega^2+D_1}\right] \tag{160}$$

Neglecting B_1 and C_1 as before, we get

$$\frac{1}{2\pi}\int_{-\infty}^{\infty}\left[\frac{\Phi_{V_T}(\omega)\Phi_{EV}(\omega)}{\Phi_{V_T}(\omega)\Phi_{EV}(\omega)}\right]d\omega = \frac{1}{2\pi}\int_{\infty}^{0}\frac{\left(2\pi\sigma_D^2\right)K_v^2\left[\omega^4\Omega^2(2\Delta^2+1-2\delta\Delta)+\omega^2\Omega^4(2\delta\Delta+\delta\Delta^3-2\Delta^2)+\Omega^6\Delta^3(\Delta^3-\delta)\right]}{(A_1\omega^4+D_1)}d\omega \tag{161}$$

Using the definite integrals in Equations 80_1, 80_2, and 80_3, and noting that A_1 is approximately equal to K_v^2, we write Equation 161 as

$$\frac{1}{2\pi}\int_{-\infty}^{\infty}\left[\frac{\Phi_{V_T}(\omega)\Phi_{EV}(\omega)}{\Phi_{V_T}(\omega)+\Phi_{EV}(\omega)}\right]d\omega = \left(2\pi\sigma_D^2\right)\left[\frac{\Omega^2(2\Delta^2+1-2\delta\Delta)}{3(D_1)^{1/6}}+\frac{\Omega^4(2\Delta+\delta\Delta^3-2\Delta^2)}{6(D_1)^{1/2}}+\frac{\Omega^6\Delta^3(\Delta^3-s)}{3(D_1)^{5/6}}\right] \tag{162}$$

Substituting for D_1 in Equation 162 gives

$$\frac{1}{2\pi}\int_{-\infty}^{\infty}\left[\frac{\Phi_{V_T}(\omega)\Phi_{EV}(\omega)}{\Phi_{V_T}(\omega)+\Phi_{EV}(\omega)}\right]d\omega \tilde{=} \left(2\pi\sigma_D^2\right)\left[\frac{\Omega^2(2\Delta^2+1-2\delta\Delta)}{(3)\Omega\Delta\left(1+2\pi\sigma_D^2/K_v^2\right)^{1/6}}\right]$$

$$+\frac{\Omega(2\Delta+\delta\Delta^3-2\Delta^2)}{6\Omega^3\Delta^3\left(1+2\pi\sigma_D^2/K_v^2\right)^{1/2}}+\frac{\Omega^6\Delta^3(\Delta^3-\delta)}{3\Omega^5\Delta^5\left(1+2\pi\sigma_D^2/K_v^2\right)^{5/6}} \qquad (163)$$

Equation 163 can be reduced to

$$\sigma^2_{DI,\,NE,\,\infty}=\frac{2\pi\sigma_D^2K^2}{3\Delta}\left[\frac{2\Delta^2+1-2\delta\Delta}{K_v^{5/3}\left(K_v^2+2\pi\sigma_D^2\right)^{1/6}}+\frac{(2+\delta\Delta^2-2\Delta)}{2\Delta K_v\left(K_v^2+2\pi\sigma_D^2\right)^{1/2}}+\frac{(\Delta^3-\delta)}{3\Delta K_v^{1/6}\left(K_v^2+2\pi\sigma_D^2\right)^{5/6}}\right] \qquad (164)$$

4.4. CALCULATION OF THE PORTION OF $\sigma^2_{DI,\,NE}$ DUE TO THE REALIZABILITY CONSTRAINT

The contribution to $\sigma^2_{DI,\,NE}$ due to the realizability constraint is of the form

$$\int_{-\infty}^{0}\left|L(t,\,T)\right|^2dt$$

where L(t, T) is given by Equation 156, repeated here:

$$L(t,\,T)=Be^{j\beta_4(t-T)}+Ce^{j\beta_5(t-T)}+De^{j\beta_6(t-T)} \qquad t<T \qquad (156)$$

Using Equations 142, 143, 144, 153, and 155 for illumination of constants β_4, β_5, β_6, β_7, B, C, and D, respectively, and also using the facts that $\beta_6=\beta_4^*$ and $D=B^*$, we reduce Equation 156 to the form

$$L(t,\,T)=\frac{1}{4}K\Omega\Delta(1-\Lambda)\left(1+\frac{1}{\Lambda}\right)^2e^{\Omega\Delta\Lambda(t-T)}+2\mathrm{Re}\left[Be^{j\beta_4(t-T)}\right] \qquad (165)$$

where the Re denotes the operation of taking the real part. After evaluation of the real part in Equation 165, we can show that L(t, T) is

$$L(t, T) = \frac{1}{4}K_v \Omega\Delta(1 - \Lambda)\left(1 + \frac{1}{\Lambda}\right)^2 e^{\Omega\Delta\Lambda(t-T)} + 2\Delta\Omega\Lambda K_v\left(1 - \frac{1}{\Lambda}\right)e^{\frac{\Omega\Delta\Lambda(t-T)}{\sqrt{2}}}\,[0.707\cos\alpha(t - T) + .866\sin\alpha(t - T)] \tag{165}_2$$

where $\alpha = \frac{\sqrt{3}}{2}\Omega\Delta\Lambda$

and where

$$L(t, T) = K_v\Omega\Delta(1 - \Lambda)\left\{\left[\frac{\Lambda + 1}{2\Lambda}\right]^2 e^{\Omega\Delta\Lambda(t-T)} - [\sqrt{2}\cos\alpha(t - T) + \sqrt{3}\sin\alpha(t - T)]e^{\frac{\Omega\Delta\Lambda(t-T)}{\sqrt{2}}}\right\} \tag{166}$$

A bold (but in this case, accurate) approximation for L(t, T) is given by

$$L(t, T) = K_v\Omega\Delta(1 - \Lambda)e^{\frac{2\Omega\Delta\Lambda(t-T)}{1+\sqrt{2}}}\left\{\left(\frac{\Lambda+1}{2\Lambda}\right)^2 - \sqrt{3}\cos[\alpha(t - T) - \theta]\right\} \tag{167}$$

where $\theta = \tan^{-1}\sqrt{3}/2$

Employing the approximation $(x + y)^2 \le 2x^2 + 2y^2$, a bound on $L^2(t, T)$ is given by

$$L^2(t, T) \le 2K_v^2\Omega^2\Delta^2(1 - \Lambda)^2 e^{\frac{4\Omega\Delta\Lambda(t-T)}{1+\sqrt{2}}}\left\{\left(\frac{\Lambda + 1}{2\Lambda}\right)^4 + 5\cos^2[\alpha(t - T) - \theta]\right\} \tag{168}$$

For purposes of establishing an upper bound, we will replace $\cos[\alpha(t - T) - \theta]$ by unity and hence obtain

$$\int_{-\infty}^{0} L^2(t, T)\,dt \le 2K_v^2\Omega^2\Delta^2(1 - \Lambda)^2\left(\frac{\Lambda + 1}{2\Lambda}\right)^4 + 5\int_{\infty}^{0} e^{\frac{4\Omega\Delta\Lambda(t-T)}{1+\sqrt{2}}}\,dt \tag{169}$$

which when evaluated yields

$$\int_{-\infty}^{0} L^2(t - T)\,dt = \frac{2K_v^2\Omega^2\Delta^2(1 - \Lambda)^2\left\{\left[\frac{\Lambda + 1}{2\Lambda}\right]^4 + 5\right\}}{(4\Omega\Delta\Lambda)/(1 + \sqrt{2})}\cdot e^{\frac{-4\Omega\Delta\Lambda T}{1+\sqrt{2}}} \tag{170}$$

which finally results in

$$\int_{-\infty}^{0} L^2(t, T)\,dt = \left(\frac{1+\sqrt{2}}{2}\right)\Omega\Delta K_v^{\,2}\Lambda\left(\frac{1-\Lambda}{\Lambda}\right)^2\left[\left(\frac{1+\Lambda}{2\Lambda}\right)^4 + 5\right]e^{-\frac{4\Omega\Delta\Lambda T}{1+\sqrt{2}}} \tag{171}$$

Finally, the minimum realizable standard deviation for filters with delay time T is found by combining Equations 171 and 164—which results in

$$\sigma^2_{DI,\,NE,\,T} = \frac{2\pi\sigma_D^{\,2}K^2}{3\Delta}\left[\frac{2\Delta^2 + 1 - 2\delta\Delta}{K_v^{5/3}\left(K_v^{\,2} + 2\pi\sigma_D^{\,2}\right)^{1/6}} + \frac{(2 + \delta\Delta^2 - 2\Delta)}{2\Delta K_v\left(K_v^{\,2} + 2\pi\sigma_D^{\,2}\right)^{1/2}} + \frac{(\Delta^3 - \delta)}{3\Delta K_v^{1/6}\left(K_v^{\,2} + 2\pi\sigma_D^{\,2}\right)^{5/6}}\right]$$

$$+\left(\frac{1+\sqrt{2}}{2}\right)\Omega\Delta K_v^{\,2}\Lambda\left(\frac{1-\Lambda}{\Lambda}\right)^2\left[\left(\frac{1+\Lambda}{2\Lambda}\right)^4 + 5\right]e^{\frac{-4\Omega\Delta\Lambda T}{1+\sqrt{2}}} \tag{172}$$

Volume II of this report will include a discussion of the theory of a pure inertial system as applied to motion compensation, and a summary of the results of the present volume.

REFERENCES

1. W. A. Porter, A Generalized Statistically Optimum Velocity-Inertial System, Report Number 2900-236-T, The University of Michigan, Institute of Science and Technology, Ann Arbor, Michigan, April 1961.
2. F. B. Berger, "The Nature of Doppler Velocity Measurement," IRE Trans., September 1957, Vol. ANE-4.
3. R. H. Cannon, "Kinematic Drift of Single-Axis Gyroscopes," Am. Soc. Mech. Engrs., New York, December 1957, Paper Number 57-A-72.
4. H. Goldstein, "Sea Echo," in C. R. Grand and B. S. Yaplee (ed.), Propagation of Short Radio Waves, McGraw-Hill, New York, N. Y., Vol. 13, Radiation Laboratory Series.
5. L. E. Goodman and A. R. Robinson, "Thermal Drift of Floated Gyroscopes," J. Appl. Mech., 1957, Vol. 24, p. 506.

BIBLIOGRAPHY

Berger, F. B., "The Design of Airborne Doppler Velocity Measuring Systems," IRE Trans., December 1957, Vol. ANE-4.

Davenport, W. B. and W. L. Root, An Introduction to the Theory of Random Signals and Noise, McGraw-Hill, New York, N. Y., 1958.

Dworetzky, L. H. and A. Edwards, "Introduction to Doppler-Inertial System Design," J. Am. Rocket Soc., December 1959.

Isaacs, R., Noise Errors in Inertial Guidance Systems, Report Number RM-483, The RAND Corp., Santa Monica, California, October 1, 1950 (CONFIDENTIAL).

James, H. M., N. B. Nichols, and R. S. Phillips, Theory of Servomechanics, McGraw-Hill, New York, N. Y., 1947.

Johnson, F., "The Synthesis of Velocity Inertial Navigation Systems," Proc. Natl. Electronics Conf., 1959.

Lanczos, C. The Variational Principles of Mechanics, University of Toronto Press, Toronto, 1957.

Lanning, J. H., and R. H. Batten, Random Processes in Automatic Control, McGraw-Hill, New York, N. Y., 1956.

Lee, Y. W. Statistical Theory of Communications, John Wiley & Sons, Inc. New York, N. Y., 1960.

Porter, W. A., and L. F. Kazda, "Optimization of a Generalized Velocity-Inertial System," IRE Trans., June 1961, Vol. ANE-8.

Strell, H., Mathematical Theory of Inertial and Doppler-Inertial Leveling, Internal Technical Memorandum Number 4619, General Precision Laboratory Inc., Pleasantville, N. Y., November 14, 1957.

Tsien, H. S., Engineering Cybernetics, McGraw-Hill, New York, N. Y., 1954.

Vowels, R. E., "The Application of Statistical Methods to Servomechanisms," Australian J. Appl. Sci., 1953, Vol. 4, pp. 469-488.

Wiener, N., Extrapolation, Interpolation and Smoothing of Stationary Time Series, Wiley, New York, N. Y., 1949.

PROJECT MICHIGAN DISTRIBUTION LIST 5
1 March 1963 — Effective Date

Copy No.	Addressee
	Commanding General U.S. Army Combat Surveillance Agency 1124 N. Highland Street Arlington 1, Virginia
2-3	Commanding General U.S. Army Electronics Command Fort Monmouth, New Jersey ATTN: AMSEL-RD
4-33	Commanding Officer U.S. Army Electronics R & D Laboratory Fort Monmouth, New Jersey ATTN: SELRA/ADT
34	Commanding General U.S. Army Electronics Proving Ground Fort Huachuca, Arizona ATTN: Technical Library
35-38	Director, U.S. Army Engineer Geodesy Intelligence & Mapping R & D Agency Fort Belvoir, Virginia
(35)	ATTN: Intelligence Division
(36)	ATTN: Research & Analysis Division
(37)	ATTN: Photogrammetry Division
(38)	ATTN: Strategic Systems Division (ENOGM-SSD)
39	Director, U.S. Army Cold Regions Research & Engineering Laboratory P. O. Box 282 Hanover, New Hampshire
40-41	Director, U.S. Army Engineers Research & Development Laboratory Fort Belvoir, Virginia ATTN: Technical Documents Center
42	Commanding Officer U.S. Army Research Office (Durham) Box CM, Duke Station Durham, North Carolina ATTN: Chief Information Processing Office
43	Assistant Commandant U.S. Army Air Defense School Fort Bliss, Texas
44	Commandant U.S. Army Engineer School Fort Belvoir, Virginia ATTN: ESSY-L
45	Commanding Officer U.S. Army Intelligence Combat Development Agency Fort Holabird Baltimore 19, Maryland
46	Commanding Officer, U.S. Army Electronic Research Unit P. O. Box 205 Mountain View, California ATTN: Electronic Defense Laboratories
47	U.S. Army Research Liaison Office MIT-Lincoln Laboratory Lexington 73, Massachusetts
48-49	Office of Naval Research Department of the Navy 17th & Constitution Avenue, N.W. Washington 25, D. C.
(48)	ATTN: Code 463
(49)	ATTN: Code 461
50	*The Hydrographer U.S. Navy Hydrographic Office Washington 25, D. C. ATTN: Code 1640
51-52	Director, U.S. Naval Research Laboratory Washington 25, D. C. ATTN: Code 2027
53	Commanding Officer U.S. Navy Ordnance Laboratory Corona, California ATTN: Library
54	Commanding Officer & Director U.S. Navy Electronics Laboratory San Diego 52, California ATTN: Library
55	Commander, U.S. Naval Ordnance Laboratory White Oak Silver Spring, Maryland ATTN: Technical Library
56-80	ASTIA (TIPCA) Arlington Hall Station Arlington 12, Virginia
81-86	Commander Wright-Patterson AFB, Ohio
(81-83)	ATTN: ASD (ASRNOO)
(84)	ATTN: ASD (ASAPR-D)
(85-86)	ATTN: ASD (ASRNGE-1)
87-89	Commander, Rome Air Development Center Griffiss AFB, New York
(87)	ATTN: RAALD
(88)	ATTN: RAWIC
(89)	ATTN: RALSS
90-94	Central Intelligence Agency 2430 E. Street, N.W. Washington 25, D. C. ATTN: OCR Mail Room
95-96	Scientific & Technical Information Facility P. O. Box 5700 Bethesda, Maryland ATTN: NASA Representative
97-98	National Aeronautics & Space Administration Manned Space Craft Center Houston 1, Texas ATTN: Chief, Technical Information Division
99	Combat Surveillance Project Cornell Aeronautical Laboratory, Incorporated P. O. Box 168 Arlington 10, Virginia ATTN: Technical Library
100	The Rand Corporation 1700 Main Street Santa Monica, California ATTN: Library
101	Research Analysis Corporation 6935 Arlington Road Bethesda, Maryland Washington 14, D. C. ATTN: Chief, Information and Control Systems Division
102-103	Cornell Aeronautical Laboratory, Incorporated 4455 Genesee Street Buffalo 21, New York ATTN: Librarian VIA: Bureau of Naval Weapons Representative 4455 Genesee Street Buffalo 21, New York

PROJECT MICHIGAN DISTRIBUTION LIST 5 (Continued)

Copy No.	Addressee
104	Columbia University Electronics Research Laboratory 632 W. 12th Street New York 27, New York ATTN: Technical Library VIA: Commander, Rome Air Development Center Griffiss AFB, New York ATTN: RCKCS
105	Coordinated Science Laboratory University of Illinois Urbana, Illinois ATTN: Librarian VIA: ONR Resident Representative 605 S. Goodwin Avenue Urbana, Illinois
106	The Ohio State University Research Foundation 1314 Kinnear Road Columbus 12, Ohio ATTN: Security Office VIA: Commander, Wright Air Development Division Wright-Patterson AFB, Ohio ATTN: ASRKSE
107-109	Jet Propulsion Laboratory California Institute of Technology 4800 Oak Grove Drive Pasadena, California VIA: NASA Western Operations Office 150 Pico Boulevard Santa Monica, California
110	Commanding Officer, U. S. Army Liaison Group Project MICHIGAN The University of Michigan P. O. Box 618 Ann Arbor, Michigan

AD

This volume deals with the optimization (for such motion-compensation activities) of a family of doppler-inertial systems. By use of the variational calculus techniques of the Wiener filter theory, functional relationships between optimum system performance and sensor noise errors are developed, and systems with and without dynamically induced errors are compared.

UNCLASSIFIED

DESCRIPTORS

Acceleration
Doppler navigation
Doppler systems
Inertial navigation
Velocity

UNCLASSIFIED

AD

This volume deals with the optimization (for such motion-compensation activities) of a family of doppler-inertial systems. By use of the variational calculus techniques of the Wiener filter theory, functional relationships between optimum system performance and sensor noise errors are developed, and systems with and without dynamically induced errors are compared.

UNCLASSIFIED

DESCRIPTORS

Acceleration
Doppler navigation
Doppler systems
Inertial navigation
Velocity

UNCLASSIFIED

AD

This volume deals with the optimization (for such motion-compensation activities) of a family of doppler-inertial systems. By use of the variational calculus techniques of the Wiener filter theory, functional relationships between optimum system performance and sensor noise errors are developed, and systems with and without dynamically induced errors are compared.

UNCLASSIFIED

DESCRIPTORS

Acceleration
Doppler navigation
Doppler systems
Inertial navigation
Velocity

UNCLASSIFIED

AD

This volume deals with the optimization (for such motion-compensation activities) of a family of doppler-inertial systems. By use of the variational calculus techniques of the Wiener filter theory, functional relationships between optimum system performance and sensor noise errors are developed, and systems with and without dynamically induced errors are compared.

UNCLASSIFIED

DESCRIPTORS

Acceleration
Doppler navigation
Doppler systems
Inertial navigation
Velocity

UNCLASSIFIED

AD Div. 19/4

Inst. of Science and Technology, Univ. of Mich., Ann Arbor
OPTIMUM CHARACTERISTICS OF SOME MOTION-COMPENSATION SYSTEMS, Volume I: Theory and Application of Doppler-Inertial Systems, by W. A. Porter, A. Y. Bilal. Mar. 63. 39 p., incl. illus., table, 5 refs.
(Report No. 2900-371-T(I))
(Contract DA-36-039 SC-78801) Unclassified report
(Project 3D5801001)

A side-looking radar system employing synthetic-antenna techniques can obtain azimuth resolution finer than that afforded by the radar beamwidth. The capabilities of such systems depend in part on the accurate sensing of vehicle perturbation from a reference path and subsequent phase compensation for this motion.

(over)

UNCLASSIFIED

I. Title: Project MICHIGAN
II. Porter, W. A., Bilal, A. Y.
III. U. S. Army Electronics Command
IV. Contract DA-36-039 SC-78801
V. Project No. 3D5801001

Armed Services Technical Information Agency
UNCLASSIFIED

AD Div. 19/4

Inst. of Science and Technology, Univ. of Mich., Ann Arbor
OPTIMUM CHARACTERISTICS OF SOME MOTION-COMPENSATION SYSTEMS, Volume I: Theory and Application of Doppler-Inertial Systems, by W. A. Porter, A. Y. Bilal. Mar. 63. 39 p., incl. illus., table, 5 refs.
(Report No. 2900-371-T(I))
(Contract DA-36-039 SC-78801) Unclassified report
(Project 3D5801001)

A side-looking radar system employing synthetic-antenna techniques can obtain azimuth resolution finer than that afforded by the radar beamwidth. The capabilities of such systems depend in part on the accurate sensing of vehicle perturbation from a reference path and subsequent phase compensation for this motion.

(over)

UNCLASSIFIED

I. Title: Project MICHIGAN
II. Porter, W. A., Bilal, A. Y.
III. U. S. Army Electronics Command
IV. Contract DA-36-039 SC-78801
V. Project No. 3D5801001

Armed Services Technical Information Agency
UNCLASSIFIED

AD Div. 19/4

Inst. of Science and Technology, Univ. of Mich., Ann Arbor
OPTIMUM CHARACTERISTICS OF SOME MOTION-COMPENSATION SYSTEMS, Volume I: Theory and Application of Doppler-Inertial Systems, by W. A. Porter, A. Y. Bilal. Mar. 63. 39 p., incl. illus., table, 5 refs.
(Report No. 2900-371-T(I))
(Contract DA-36-039 SC-78801) Unclassified report
(Project 3D5801001)

A side-looking radar system employing synthetic-antenna techniques can obtain azimuth resolution finer than that afforded by the radar beamwidth. The capabilities of such systems depend in part on the accurate sensing of vehicle perturbation from a reference path and subsequent phase compensation for this motion.

(over)

UNCLASSIFIED

I. Title: Project MICHIGAN
II. Porter, W. A., Bilal, A. Y.
III. U. S. Army Electronics Command
IV. Contract DA-36-039 SC-78801
V. Project No. 3D5801001

Armed Services Technical Information Agency
UNCLASSIFIED

AD Div. 19/4

Inst. of Science and Technology, Univ. of Mich., Ann Arbor
OPTIMUM CHARACTERISTICS OF SOME MOTION-COMPENSATION SYSTEMS, Volume I: Theory and Application of Doppler-Inertial Systems, by W. A. Porter, A. Y. Bilal. Mar. 63. 39 p., incl. illus., table, 5 refs.
(Report No. 2900-371-T(I))
(Contract DA-36-039 SC-78801) Unclassified report
(Project 3D5801001)

A side-looking radar system employing synthetic-antenna techniques can obtain azimuth resolution finer than that afforded by the radar beamwidth. The capabilities of such systems depend in part on the accurate sensing of vehicle perturbation from a reference path and subsequent phase compensation for this motion.

(over)

UNCLASSIFIED

I. Title: Project MICHIGAN
II. Porter, W. A., Bilal, A. Y.
III. U. S. Army Electronics Command
IV. Contract DA-36-039 SC-78801
V. Project No. 3D5801001

Armed Services Technical Information Agency
UNCLASSIFIED

AD Div. 19/4

Inst. of Science and Technology, Univ. of Mich., Ann Arbor
OPTIMUM CHARACTERISTICS OF SOME MOTION-COMPENSATION SYSTEMS, Volume I: Theory and Application of Doppler-Inertial Systems, by W. A. Porter, A. Y. Bilal. Mar. 63. 39 p., incl. illus., table, 5 refs.
(Report No. 2900-371-T(I))
(Contract DA-36-039 SC-78801) Unclassified report
(Project 3D5801001)

A side-looking radar system employing synthetic-antenna techniques can obtain azimuth resolution finer than that afforded by the radar beamwidth. The capabilities of such systems depend in part on the accurate sensing of vehicle perturbation from a reference path and subsequent phase compensation for this motion.

(over)

UNCLASSIFIED

I. Title: Project MICHIGAN
II. Porter, W. A., Bilal, A. Y.
III. U. S. Army Electronics Command
IV. Contract DA-36-039 SC-78801
V. Project No. 3D5801001

Armed Services
Technical Information Agency
UNCLASSIFIED

AD Div. 19/4

Inst. of Science and Technology, Univ. of Mich., Ann Arbor
OPTIMUM CHARACTERISTICS OF SOME MOTION-COMPENSATION SYSTEMS, Volume I: Theory and Application of Doppler-Inertial Systems, by W. A. Porter, A. Y. Bilal. Mar. 63. 39 p., incl. illus., table, 5 refs.
(Report No. 2900-371-T(I))
(Contract DA-36-039 SC-78801) Unclassified report
(Project 3D5801001)

A side-looking radar system employing synthetic-antenna techniques can obtain azimuth resolution finer than that afforded by the radar beamwidth. The capabilities of such systems depend in part on the accurate sensing of vehicle perturbation from a reference path and subsequent phase compensation for this motion.

(over)

UNCLASSIFIED

I. Title: Project MICHIGAN
II. Porter, W. A., Bilal, A. Y.
III. U. S. Army Electronics Command
IV. Contract DA-36-039 SC-78801
V. Project No. 3D5801001

Armed Services
Technical Information Agency
UNCLASSIFIED

AD Div. 19/4

Inst. of Science and Technology, Univ. of Mich., Ann Arbor
OPTIMUM CHARACTERISTICS OF SOME MOTION-COMPENSATION SYSTEMS, Volume I: Theory and Application of Doppler-Inertial Systems, by W. A. Porter, A. Y. Bilal. Mar. 63. 39 p., incl. illus., table, 5 refs.
(Report No. 2900-371-T(I))
(Contract DA-36-039 SC-78801) Unclassified report
(Project 3D5801001)

A side-looking radar system employing synthetic-antenna techniques can obtain azimuth resolution finer than that afforded by the radar beamwidth. The capabilities of such systems depend in part on the accurate sensing of vehicle perturbation from a reference path and subsequent phase compensation for this motion.

(over)

UNCLASSIFIED

I. Title: Project MICHIGAN
II. Porter, W. A., Bilal, A. Y.
III. U. S. Army Electronics Command
IV. Contract DA-36-039 SC-78801
V. Project No. 3D5801001

Armed Services
Technical Information Agency
UNCLASSIFIED

AD Div. 19/4

Inst. of Science and Technology, Univ. of Mich., Ann Arbor
OPTIMUM CHARACTERISTICS OF SOME MOTION-COMPENSATION SYSTEMS, Volume I: Theory and Application of Doppler-Inertial Systems, by W. A. Porter, A. Y. Bilal. Mar. 63. 39 p., incl. illus., table, 5 refs.
(Report No. 2900-371-T(I))
(Contract DA-36-039 SC-78801) Unclassified report
(Project 3D5801001)

A side-looking radar system employing synthetic-antenna techniques can obtain azimuth resolution finer than that afforded by the radar beamwidth. The capabilities of such systems depend in part on the accurate sensing of vehicle perturbation from a reference path and subsequent phase compensation for this motion.

(over)

UNCLASSIFIED

I. Title: Project MICHIGAN
II. Porter, W. A., Bilal, A. Y.
III. U. S. Army Electronics Command
IV. Contract DA-36-039 SC-78801
V. Project No. 3D5801001

Armed Services
Technical Information Agency
UNCLASSIFIED

AD

This volume deals with the optimization (for such motion-compensation activities) of a family of doppler-inertial systems. By use of the variational calculus techniques of the Wiener filter theory, functional relationships between optimum system performance and sensor noise errors are developed, and systems with and without dynamically induced errors are compared.

UNCLASSIFIED

DESCRIPTORS

Acceleration
Doppler navigation
Doppler systems
Inertial navigation
Velocity

UNCLASSIFIED

AD

This volume deals with the optimization (for such motion-compensation activities) of a family of doppler-inertial systems. By use of the variational calculus techniques of the Wiener filter theory, functional relationships between optimum system performance and sensor noise errors are developed, and systems with and without dynamically induced errors are compared.

UNCLASSIFIED

DESCRIPTORS

Acceleration
Doppler navigation
Doppler systems
Inertial navigation
Velocity

UNCLASSIFIED

AD

This volume deals with the optimization (for such motion-compensation activities) of a family of doppler-inertial systems. By use of the variational calculus techniques of the Wiener filter theory, functional relationships between optimum system performance and sensor noise errors are developed, and systems with and without dynamically induced errors are compared.

UNCLASSIFIED

DESCRIPTORS

Acceleration
Doppler navigation
Doppler systems
Inertial navigation
Velocity

UNCLASSIFIED

AD

This volume deals with the optimiza r such motion-compensation activities) of a family ler-inertial systems. By use of the variational ca chniques of the Wiener filter theory, functional relations..ps between optimum system performance and sensor noise errors are developed, and systems with and without dynamically induced errors are compared.

UNCLASSIFIED

DESCRIPTORS

Acceleration
Doppler navigation
Doppler systems
Inertial navigation
Velocity

UNCLASSIFIED

UNCLASSIFIED